RESEARCH ARTICLE

Robust and replicable effects of ageing on resting-state brain electrophysiology measured with MEG

Andrew J Quinn[1]*, Jemma Pitt[2,3], Oliver Kohl[4], Chetan Gohil[2], Mats WJ van Es[2], Anna C Nobre[2,5,6,7], Mark W Woolrich[2]

[1]Centre for Human Brain Health, School of Psychology, University of Birmingham, Birmingham, United Kingdom; [2]Oxford Centre for Human Brain Activity, Wellcome Centre for Integrative Neuroimaging, Department of Psychiatry, University of Oxford, Oxford, United Kingdom; [3]Institute of Cognitive Neuroscience, University College London, London, United Kingdom; [4]Institute of Clinical Neuroscience and Medical Psychology, Medical Faculty and University Hospital Düsseldorf, Heinrich Heine University, Düsseldorf, Germany; [5]Department of Experimental Psychology, University of Oxford, Oxford, United Kingdom; [6]Wu Tsai Institute, Yale University, New Haven, United States; [7]Department of Psychology, Yale University, New Haven, United States

***For correspondence:** a.quinn@bham.ac.uk

Competing interest: The authors declare that no competing interests exist.

Funding: See page 23

Preprint posted
18 September 2025
Sent for Review
07 October 2025
Reviewed preprint v1
09 December 2025
Reviewed preprint v2
13 August 2026
Version of Record
12 October 2026

Reviewing Editor: Redmond G O'Connell, Trinity College Dublin, Ireland

© Copyright Quinn *et al.* This article is distributed under the terms of the Creative Commons Attribution License, which permits unrestricted use and redistribution provided that the original author and source are credited.

eLife Assessment

The authors ask whether a simple whole-head spectral power analysis of human magnetoencephalography data recorded at rest in a large cohort of adults shows robust effects of age, and their results provide **compelling** evidence that it does. The relative simplicity of the analysis is a major strength of the paper, and the authors are careful to control for many different confounds - although perhaps highly correlated factors like brain anatomy still pose a slight issue. The paper provides a **valuable** power analysis framework that should inform researchers across the broader neuroimaging community.

Abstract Non-invasive recordings of brain electrophysiology provide credible insights into decline in neuronal functioning with age. New approaches are required to translate these results into compelling clinical metrics and meet the global challenge of preserving brain health in ageing. Changes in neuronal dynamics with ageing are observable in the power spectra of EEG and MEG recordings. Highly promising candidates for electrophysiological markers have been identified, but progress is hindered by substantial methodological variability across studies. This makes it challenging to establish a clear consensus on the frequency, location, and direction of any single reported effect within the larger body of research. We estimate a full-frequency whole-head profile of the ageing effect on eyes-closed resting-state MEG using the GLM-Spectrum. This data representation is easily sharable, facilitates meta-analyses, and provides a framework for estimating statistical power of age effects for future study planning. We use this to show that the effect of age replicates across open-access MEG datasets and is robust to modelling of common covariates. Distinct components within the full-frequency profile have different effect sizes, indicating that sample-size planning for ageing effects must consider the specific features of interest. The frequency profile of ageing is strongly robust to a range of common covariates and partially robust to modelling of grey matter volume. We establish that what seems a well-powered study may become underpowered when analyses target an age effect that is linearly separable from an age-relevant covariate such as

grey matter volume. These results provide a pathway towards formal comparison and assessment of candidate markers for brain health in ageing.

Introduction

Ageing is a major risk factor for a wide range of major pathologies of the brain (***López-Otín et al., 2013***), including neurodegenerative disorders (***Planche et al., 2022***) and stroke (***Ellekjær et al., 1997***; ***Feigin et al., 2014***). Changes in human brain electrophysiology are observable through changes in the power spectrum of electromagnetic fields measured by EEG and MEG. These approaches offer a direct perspective on temporal synchronization of neuronal activity (***Babiloni et al., 2020***). This synchronization depends on the integrity of network connections and is known to degrade throughout the ageing process (***Maestú and Fernández, 2020***). Such effects have been observed in the neuronal power spectrum of both MEG (***Brady et al., 2020***; ***Gómez et al., 2013***; ***Hoshi and Shigihara, 2020***; ***Rempe et al., 2023***; ***Stier et al., 2023***; ***Osipova et al., 2005***; ***Hughes et al., 2019***) and EEG recordings (***Klimesch, 1999***; ***Park et al., 2024***; ***Turner et al., 2023***; ***Zibrandtsen and Kjaer, 2021***). Non-invasive measures of brain electrophysiology are a highly promising approach to contribute towards the global aim of allowing more people to realise their potential across the full lifespan (***World Health Organization, 2015***).

Electrophysiological signatures of ageing across studies in the literature are diverse, or even conflicting. It can be challenging to reconcile differences across differing analysis choices, frequency bands, and brain regions (***Donoghue et al., 2021***). For example, increasing age has a longstanding association with a reduction in posterior alpha band (7–13 Hz) power (***Klimesch, 1999***). Yet, the broader literature reveals that this effect varies in magnitude and may even reverse direction across brain regions, frequency bands, and analysis pipelines (***Gómez et al., 2013***; ***Hoshi and Shigihara, 2020***; ***Lodder and van Putten, 2011***; ***Park et al., 2024***; ***Pathak et al., 2022***; ***Quinn et al., 2024***; ***Rempe et al., 2023***; ***Scally et al., 2018***; ***Zibrandtsen and Kjaer, 2021***, see Appendix 1 for a summary of effects of alpha power and age.). Credible scientific claims must be supported by evidence of replicability in new datasets and robustness to reasonable variations in analysis (***Botvinik-Nezer and Wager, 2023***; ***Nosek and Errington, 2020***; ***Nosek et al., 2022***), but our ability to integrate results across studies is hindered by the large variety of analytic choices used in the literature. This makes it difficult to synthesize findings from multiple datasets, either as a manual comparison or a formal meta-analysis.

Neuroscience researchers working on MRI facilitate comparability and meta-analyses by computing and distributing whole-volume statistical maps along with results of individual studies (***Gorgolewski et al., 2015***). A similar approach is possible for spectral analysis of MEG/EEG, e.g., computing and sharing full-frequency and whole-head estimates of critical effects without binning results into frequency bands or regions of interest. Features such as canonical frequency bands may be a useful guide for interpretation of results, but they can oversimplify the profile of the underlying spectrum and add a source of variability between studies that can prevent aggregation of results. Reporting of whole-head and full-frequency spectra of effect estimates would make it straightforward to aggregate across studies and eventually enable identification of sub-threshold effects that may be missed in single analyses but are consistent across studies. We argue that this approach provides a generalisable foundation that can support more complex analyses that have a frequency component (such as aperiodic slopes, burst detection, and dynamic functional networks) that require more researcher degrees of freedom.

Effect sizes are another essential tool for comparing and aggregating results across studies. They quantify the magnitude or practical significance of an estimated effect without reducing it to a hypothesis test with a binary outcome that might be dependent on practical factors such as sample size (***Smith and Nichols, 2018***). Critically, effect sizes allow efficient use of data by supporting planning for future data samples through power analyses. Statistically underpowered studies are more likely to lead to incorrect conclusions and inaccurate estimates of effect sizes when all other aspects of experimental design and analysis have been conducted perfectly (***Button et al., 2013***; ***Cremers et al., 2017***). This is critical for neuroimaging analyses where different spatial, temporal, or spectral components of the same signal feature can have different effect sizes (***Baker et al., 2021***). Many

guidelines on good practice in electrophysiology research encourage reporting effect sizes (***Gross et al., 2013***; ***Hillebrand et al., 2018***; ***Baker et al., 2021***) though this remains relatively uncommon in electrophysiology.

Here, we use a GLM-Spectrum (***Quinn et al., 2024***) approach to quantify and visualise age effects in the Cam-CAN dataset (***Shafto et al., 2020***). The method uses multiple regression to model the relationships between multiple explanatory variables and the oscillatory power at each spatial location and frequency bin. The approach is expanded with between-subject effect size estimation in addition to replication on multiple datasets. An additional exploration examines how the age effect is changed when including other covariates in the model. The results are discussed in the context of the wider literature on age effects and lay the groundwork for rigorous evaluation and benchmarking of potential biomarkers for brain health in ageing.

Results

We first quantify the change in the MEG frequency spectrum across the adult lifespan using the Cam-CAN dataset in section 'A whole-head and full-frequency depiction of age-related change to the neuronal power spectrum'. Section 'Effect size of age is variable across space and frequency, with consequences for sample size planning' explores the effect sizes of the adult lifespan results and section 'Quadratic effects of age' expands these approaches to explore quadratic 'U' shaped effects of age. Section 'Sample size planning for effects of age on the neuronal power spectrum' provides bootstrapped estimates of effect sizes to compute sample size guidance for planned replications of our results. We next demonstrate the reproducibility of these results across several MEG-UK datasets in section 'The spectral profile of age effects on brain electrophysiology is replicable across datasets' and their robustness across analyses that control for a range of potential confounding variables in sections 'The robustness of the age effect to head position correction' and 'Between-participant covariates mediate the age effect differently across the spectrum'. Finally, we quantify the impact of including grey matter volume as a covariate on the effect size of the age effect in section 'Isolating the component of the age effect on brain electrophysiology that is distinct from global reduction in grey

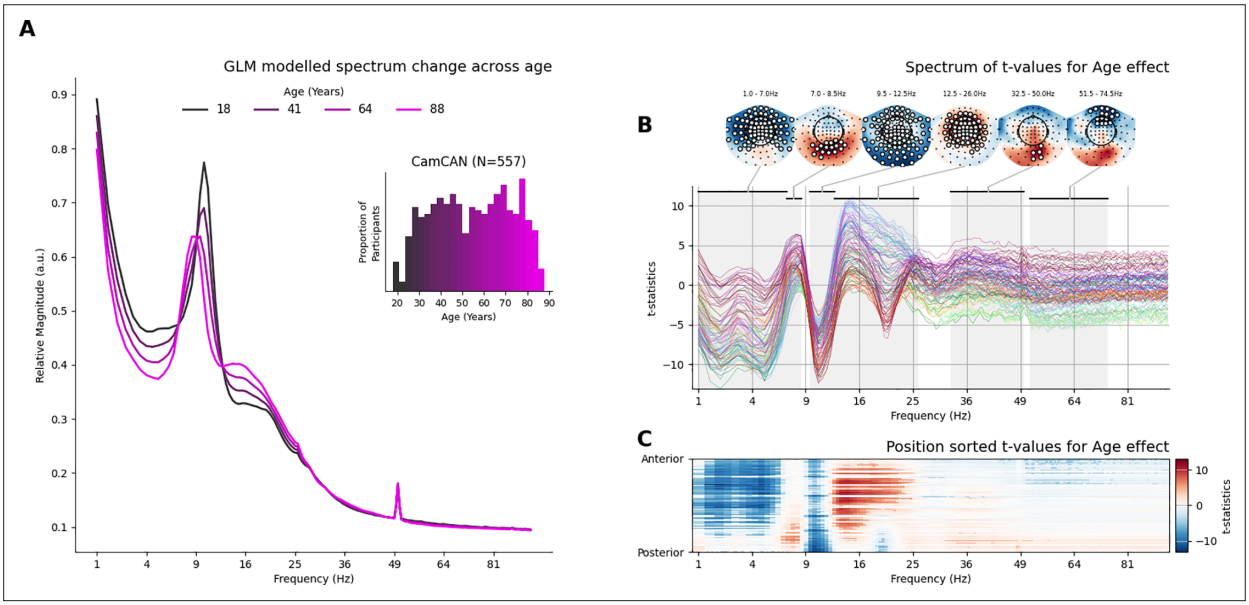


Figure 1. Effect of age on the relative magnitude spectrum across space and frequency. (**A**) Model-predicted spectra (averaged across all sensors) for four equally spaced ages across the participant age range with inset histogram of participant ages within Cam-CAN. (**B**) Spectrum of t-values quantifying the age effect across space and frequency. Non-parametric permutations with maximum statistics to control for multiple comparisons across sensors and frequency bins. While this permutation testing was not cluster-based, contiguous clusters of significant sensors were computed post hoc for visualisation. The largest six spatially and spectrally contiguous areas of statistically significant effects are highlighted in frequency by black bands at the top of the spectrum and highlighted in space by sensors marked with a white circle in the adjoining topography. (**C**) A 2D frequency-by-space map of all statistically significant effects. Sensor-frequency combinations that do not reach statistical significance have a faded colour scale. Blue regions indicate decreasing spectral power with age and red regions indicate increases.

matter volume'. A summary of all GLM analyses carried out in this work is available in ***Appendix 7—table 1***.

A whole-head and full-frequency depiction of age-related change to the neuronal power spectrum

MEG data from Cam-CAN (***Shafto et al., 2020***) for 557 participants during eyes-closed resting state were analysed. After data pre-processing and cleaning, a two-level GLM-Spectrum (***Quinn et al., 2024***) approach was used to characterise the average magnitude and the linear slope effect of age across the spectrum for each sensor. ***Figure 1A*** uses the estimated GLM-Spectrum coefficients to show the model prediction of how the spectrum changes across age. This shows a characteristic pattern that combines a variety of previously reported results into a single analysis. Importantly, these effects are continuous across the spectrum and would be challenging to objectively unpick without a full-spectrum approach.

The t-statistic spectrum (***Figure 1B***) is the test statistic for the linear effect of age at each point in frequency for each sensor. A positive t-value indicates that power in that frequency bin at that sensor position increases with age and vice versa for negative t-values. The statistical significance of the t-statistic spectrum of the age-effect (i.e. rejecting the hypothesis that there is no age effect) was computed using non-parametric permutations with maximum statistics to control for multiple comparisons across sensors and frequency bins. While this permutation testing was not cluster-based, contiguous clusters of significant sensors were computed post hoc for visualisation. ***Figure 1B*** shows the t-value spectrum of the age with the largest post hoc clusters overlaid and ***Figure 1C*** shows the effect organised into a 2D image across space (anterior to posterior) and frequency as a statistical parametric map (***Litvak et al., 2011***). The 2D image representation simplifies visualisation as it does not rely on colour coding of sensor location. Critically, both the t-statistic spectrum and 2D image are simple visualisations of the age effect that allow statistically significant and sub-threshold effects to be shared and reused in the literature.

The maximum-statistic permutations testing results identified a broad set of effects, including six contiguous regions within the age-effect spectrum (***Figure 1B***). Firstly, older adults have lower spectral magnitude than young adults at low frequencies (<7 Hz). This is a spatially broad effect that peaks in central/frontal regions. This analysis does not separate different effects in low-frequency bands such as delta and theta. Rather, they appear as a contiguous effect that spreads across the whole 1–7 Hz range. Older adults have relatively high magnitude around 7–8.5 Hz, and younger adults have higher magnitude around 9.5–12.5 Hz. Both effects peak in posterior/occipital regions, with the negative age effect at higher frequencies spreading more widely across the sensor array. These effects are visible as distinct peaks with opposite direction (***Figure 1B***) in the GLM-Spectrum of the age effect. Referring to the model predicted spectra (***Figure 1A***) suggests that this may reflect a slowing of the alpha peak frequency. Older adults have higher spectral magnitude between 12.5 and 26 Hz in central/motor regions corresponding to sensorimotor band activity. Finally, two effects are identified with centre frequencies above 30 Hz. Older adults have higher relative magnitude in posterior central sensors at frequencies between 32.5 and 50 Hz and have lower relative magnitude in fronto-central regions in the gamma region between 51.5 and 80 Hz (frequencies above 100 Hz were not included in the model).

We have completed several control analyses to support these findings. Firstly, we have explored the qualitative correspondence between alpha peak frequency and the two effects we identified within the canonical alpha range (see Appendix 1). Secondly, the overall pattern of findings is consistent in an equivalent source space analysis using LCMV beamforming and parcellation (see Appendix 2). Finally, we have repeated the analyses with and without ICA denoising and find that the overall spectral profile is very similar. Effects in low-frequencies, low-alpha, and high-gamma are increased with application of ICA, whilst high-alpha and beta remain unchanged, and low-gamma effects are reduced (see Appendix 3).

Effect size of age is variable across space and frequency, with consequences for sample size planning

Neuroimaging analyses, such as the results in ***Figure 1*** , typically focus on testing hypotheses about the presence of effects in brain imaging data, not estimating their magnitude. These hypothesis tests are

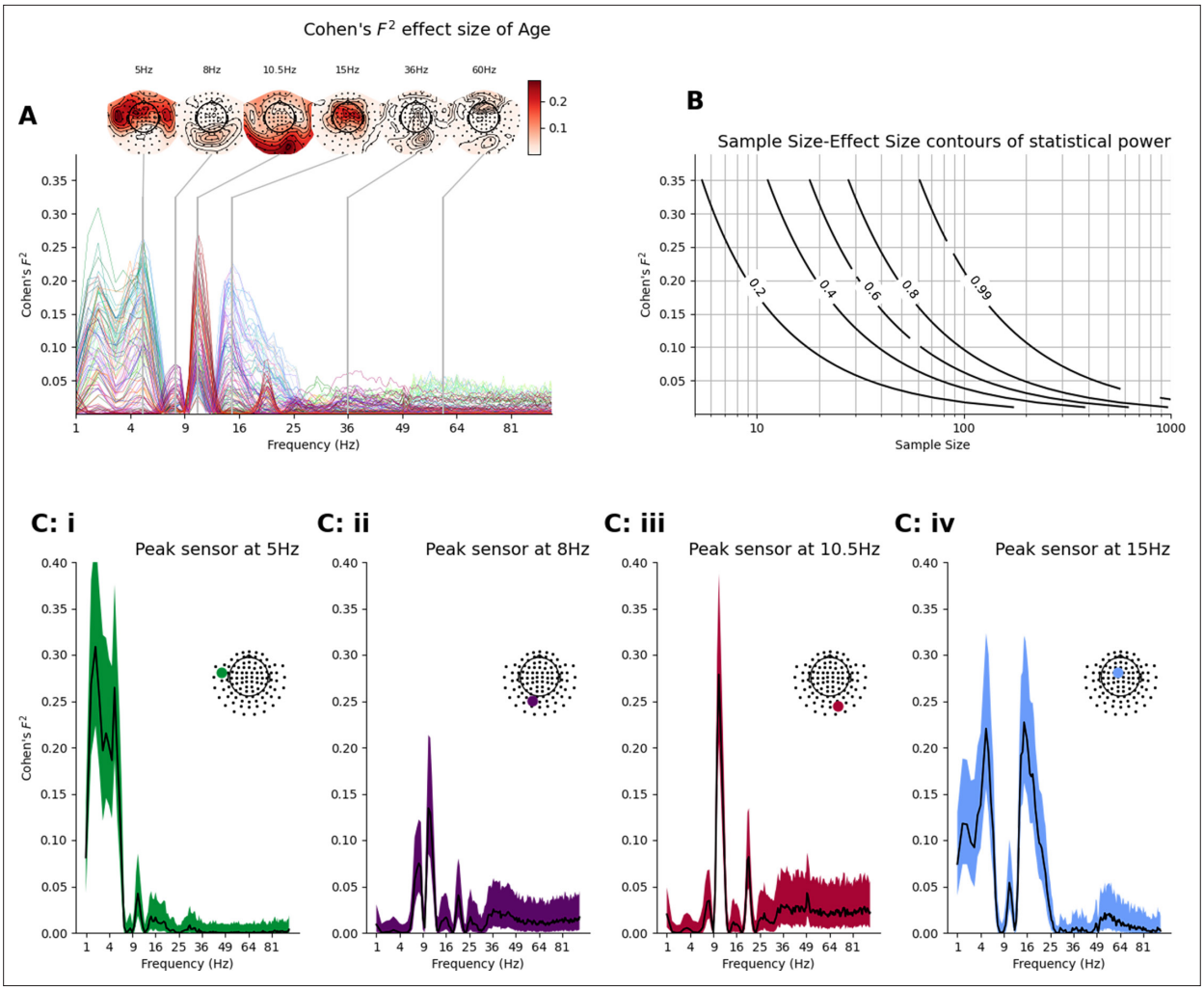


Figure 2. Cohen's F^2 effect size for the linear effect of age. (**A**) Cohen's F^2 effect size for age across space and frequency. Each line is a sensor, with a colour matched to the sensors in the topography shown in the inset. The six topographies show spatial distributions across the sensor array at the peak frequency of the six significant effects identified in ***Figure 1B***. (**B**) Contours showing the relationship between effect size and sample size for five different experimental power levels. As sample sizes get larger, there is sufficient power to reliably detect smaller effect sizes. (**C**) Effect size spectra with bootstrapped 95% confidence intervals at the peak sensor for the four largest effects identified in ***Figure 1B***.

sample-size dependent, so that practically insignificant effects may become significant in sufficiently large datasets. Effect sizes estimate the strength of a phenomenon or relationship, independently of sample size. They better reflect an effect's importance in a clinical or behavioural context (***Reddan et al., 2017***) and can be used as a basis for power analysis (i.e. sample size planning) to inform future research. In this analysis, the effect size of the age regressor within the GLM-Spectrum was computed using Cohen's F^2 (***Cohen, 1988***; ***Selya et al., 2012***) for each sensor and frequency bin in the analysis. Cohen's F^2 corresponds to the proportion of variance in the data that is uniquely explained by an explanatory variable (i.e. regressor) of interest within the context of a multiple regression model.

The spectrum of effect sizes for the age regressor (***Figure 2A***) indicates the strength or practical impact of ageing on the spectrum. The effect size spectrum contains local peaks that correspond to the effects highlighted in section 'A whole-head and full-frequency depiction of age-related change to the neuronal power spectrum'. The largest effects with local peaks at 5 Hz, 8 Hz, 10.5 Hz, 15 Hz, 36 Hz, and 60 Hz have close spatial and spectral correspondence to extrema in the t-spectrum in ***Figure 1B***. Low-frequency, upper alpha and beta range results show effect sizes peaking between $F^2 = 0.2$ to $F^2 = 0.3$, indicating that ageing had a relatively large practical impact on the spectrum in these bands. In contrast, though they achieved statistical significance in the hypothesis tests (***Figure 1***), lower alpha and the gamma results had effect sizes around $F^2 \leq 0.075$, indicating a relatively small practical

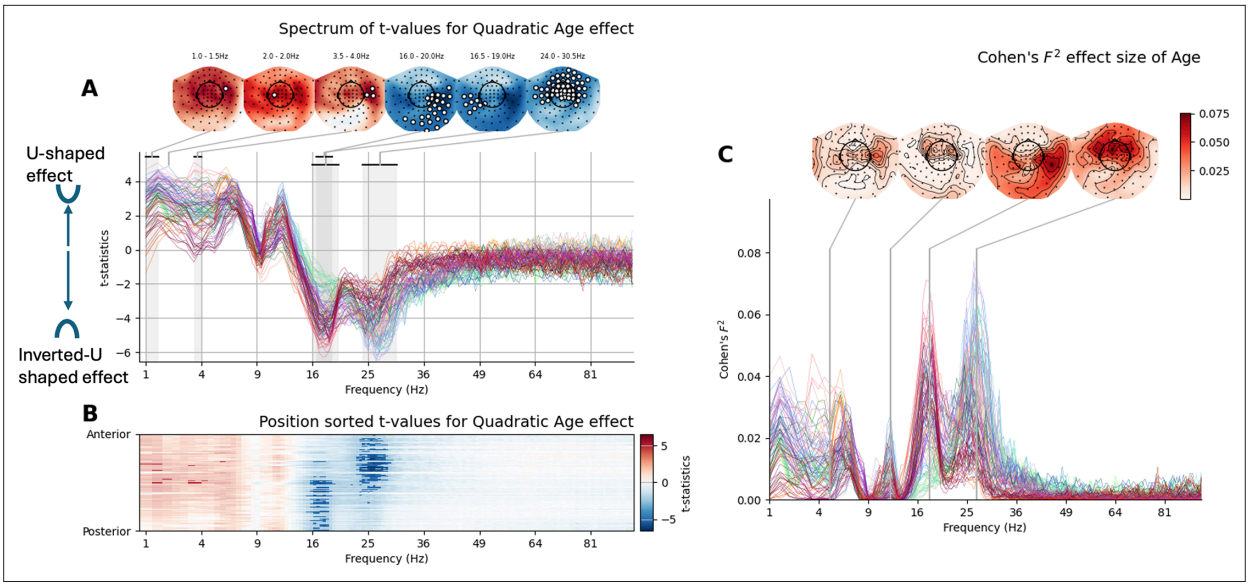


Figure 3. Quadratic effects of age on the neuronal frequency spectrum. (**A**) The spectrum of t-values for the quadratic effect of age for all frequencies and channels. Positive values indicate a 'U' shaped effect and negative values indicate an 'inverted-U' shaped effect. Shaded regions and sensors indicated on the topomaps indicate statistical significance identified using non-parametric permutations with maximum-statistic correction for multiple comparisons. (**B**) A 2D frequency-by-space map of all statistically significant effects. Sensor-frequency combinations that do not reach statistical significance have a faded colour scale. Blue regions indicate inverted-U shaped effects of age and red regions indicate U shaped effects. (**C**) The spectrum of effect sizes for the quadratic effects of age.

impact of ageing on the spectrum. These effect sizes can be used to construct sample size estimates to inform future study planning. Power contours (***Baker et al., 2021***) across different effect sizes and sample sizes can provide a visual guide to the number of participants required to achieve a given statistical power in a future replication of the present analyses (***Figure 2B***).

It is important to acknowledge that effect sizes are estimates themselves and can vary in their precision depending on the dataset and analysis. To quantify this variability, bootstrapped confidence intervals were computed for each sensor and frequency pair. The computed confidence limits of the effect size estimates vary substantially across sensors and frequencies. (***Figure 2C*** shows the effect sizes with confidence intervals at the peak sensor for the first four significant effects.)

Quadratic effects of age

The linear effect of age is a convenient and simple regression model. However it makes a strong assumption that change with age is uniform across the whole age range. A second group-level GLM was computed with an additional regressor to quantify quadratic effects of age, which have been reported in the ageing literature (***Gómez et al., 2013***; ***Rempe et al., 2023***; ***Stier et al., 2023***). The spectrum of t-values for the quadratic age predictor (***Figure 3***) shows significant effects for a U-shaped change with increasing age in the low-frequency (1–5 Hz) range in central sensors. Significant inverted-U shaped effects are present in two frequency ranges in the beta band. A low-frequency beta effect is present in occipital and temporal sensors between 16 and 20 Hz, whilst a second high-beta effect is present in central sensors between 24 and 30.5 Hz. The low-frequency and low-beta effects overlap in space and frequency with linear effects, suggesting that the low-frequency change with age has both a linear increase with age and a U-shaped component, whilst the low-beta effect has a decrease with age and an inverted-U shaped component. The high-beta effect does not overlap in frequency with any of the reported linear effects. The effect sizes for quadratic effects range between Cohen's F^2 values of 0.033 for low frequency to 0.076 for high beta and are generally lower than the effect sizes for linear change.

Table 1. Summary of significant spatio-spectral regions containing an age effect in Cam-CAN.
The estimated sample sizes are the range of sample sizes needed to have an 80% chance of detecting the effect in a future sample, assuming that both the effects here are true and that the effect sizes are well estimated. Sample size ranges are computed from bootstrapped 95% confidence intervals for effect size estimate. The lower bound of the 95% confidence intervals can be taken as a smallest effect size of interest. The sample size forecasts are not informative about the present results and serve only as a guide for future study planning.

Descriptive label	Peak freq (range)	Peak t-value	Peak region	Peak Cohen's F^2 (95% CI)	Estimated future sample for 80% power
Linear effects					
Low freq	5 Hz (1–7)	–12.11	Frontal	0.264 (0.187–0.375)	26–51
Low alpha	8 Hz (7–8.5)	+6.44	Occipital	0.074 (0.044–0.122)	79–218
High alpha	10.5 Hz (9.5–12.5)	–12.43	Occipito-parietal	0.278 (0.205–0.387)	25–47
Beta	15 Hz (12.5–26)	+11.22	Central	0.227 (0.162–0.320)	30–60
Low gamma	36 Hz (32.5–50)	+5.77	Occipital	0.06 (0.030–0.111)	86–315
High gamma	60 Hz (51.5–74.5)	–5.37	Frontal	0.052 (0.024–0.098)	97–396
Quadratic effects					
Left beta	17 (16.5–17)	–4.62	LH occipito-temporal	0.033 (0.036–0.11)	82–264
Right beta	18 (16 - 20)	–6.26	RH occipito-temporal	0.071 (0.044–0.13)	76–222
Central high beta	27 (24–30.5)	–6.47	Anterior central	0.076 (0.044–0.12)	80–218

Sample size planning for effects of age on the neuronal power spectrum

We use the 95% confidence intervals around the effect sizes to make recommendations for future sample sizes for future samples that plan to replicate these results. The observed power calculations have no bearing on the interpretation of the present results. Instead, they should be used as a general guideline for planning future studies. ***Table 1*** gives a full summary of the peak statistics and future sample size range for the age effects identified in ***Figure 1B*** and ***Figure 3A***. These results have implications for future sample planning for resting-state electrophysiology studies of ageing. Using the upper bound of the sample size estimates as a conservative estimate, the linear changes with age that have relatively large effect sizes would have well-powered replications with sample sizes of around 50–60 participants. However, the smaller linear effects and all the quadratic effects would require samples of 200 or more participants to have the same probability of detecting the effect if it is indeed present (***Table 1***). This indicates that study samples should be planned with the smallest effect of interest in mind and that ageing effects in different frequency bands may not all be well powered within the same sample.

The spectral profile of age effects on brain electrophysiology is replicable across datasets

To explore the replicability of the ageing effect reported from the Cam-CAN dataset, the analysis was repeated on eyes-closed resting-state recordings from three smaller datasets from the MEG-UK database (https://meguk.ac.uk/database/). Replicability was quantified by the correlation of the whole spectral profile of the age effect between datasets. We have only completed the replication analysis with the linear effects of age as the quadratic effects from Cam-CAN have smaller effect sizes that indicate that the MEG-UKI datasets may not be able to detect these effects based on their sample size.

Overall, the spectral profile of the ageing effect is highly replicable across MEG datasets acquired on different systems and across different facilities. We identified high correlations between the spectral profiles of the age parameter estimates, inferential statistics, and effect sizes in each of the four datasets (***Figure 4***). In particular, the spectral profiles for the parameter estimates and t-statistics were strikingly similar across datasets (Pearson's *r* between 0.67 and 0.97 for parameter estimates and

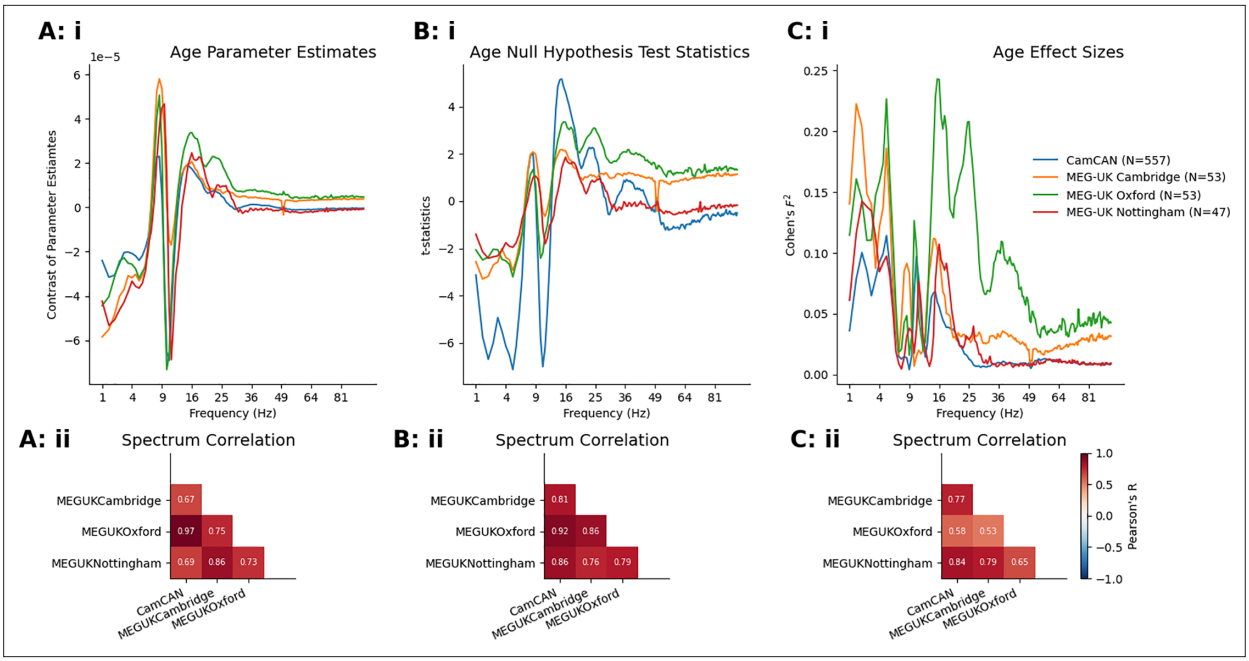


Figure 4. Replicability of the parameter estimates, t-statistics, and effect sizes of ageing on the neuronal power spectrum. (**Ai**) Spectrum of parameter estimates across frequency (averaged over all sensors) for each of the four datasets. (**Aii**) Correlation matrix indicating similarity of the sensor-averaged frequency profile of the age effect between datasets. (**Bi and Bii**) As (A) for null hypothesis test statistics. (**Ci and Cii**) As (A) for effect sizes.

between 0.76 and 0.92 for t-statistics), suggesting a high level of replicability. The spectral profile of effect sizes was also positively correlated across datasets but to a lesser extent (Pearson's *r* between 0.53 and 0.84). Maximum and minimum t-statistics for Cam-CAN are substantially larger in magnitude than in the smaller MEG-UK datasets. This is an expected consequence of the larger sample size of Cam-CAN on null-hypothesis test statistics such as t-values.

The topography of age-related change is qualitatively reproduced across all datasets (***Figure 5A***) with some variability in the extent and spread of effects in specific datasets. Whilst the lower-frequency effects are highly consistent, there is more variability in the higher-frequency effects (>30 Hz), which can change direction across participants (***Figure 5B, C, D***). The smaller data samples have more variable estimates for Cohen's F^2 when compared to Cam-CAN. Whilst the interpretation of effect sizes doesn't rely on reaching a predetermined significance threshold, they do depend on having enough data to be considered reliable. This is reflected in the greater variability in effect sizes seen in the smaller data samples. The overall profiles of Cohen's F^2 are similar across datasets, yet the peak effect size in the low-frequency and beta ranges can still vary by a factor of two or three between data samples. This may arise from relatively poor estimates of the population-level variability from smaller data samples. It is possible that more systematic differences in the participant sampling, recruitment, and data acquisition process could contribute to between-site differences. At present, our analyses can show that the core effects of ageing are replicable across several datasets, though we have not formally combined these datasets into a single analysis. Formal methods for data harmonisation, such as ComBat (***Johnson et al., 2007***), could correct for additive and multiplicative differences in data scaling across sites to improve site comparisons.

The robustness of the age effect to head position correction

The results so far have looked at age effects on the relative spectral magnitude of each frequency compared to the sum across frequencies. Whilst the absolute spectral magnitude is simpler to interpret in terms of underlying neuronal activity, it can be confounded by the position of the participant relative to the MEG sensors (some sensors will be closer to neuronal source than others) and by inter-individual variability in this position (***Gross et al., 2013***). It is common to apply a correction or normalisation to sensor-space analyses to control for these effects, though this is an impactful decision which can change the profile of effects seen in the results.

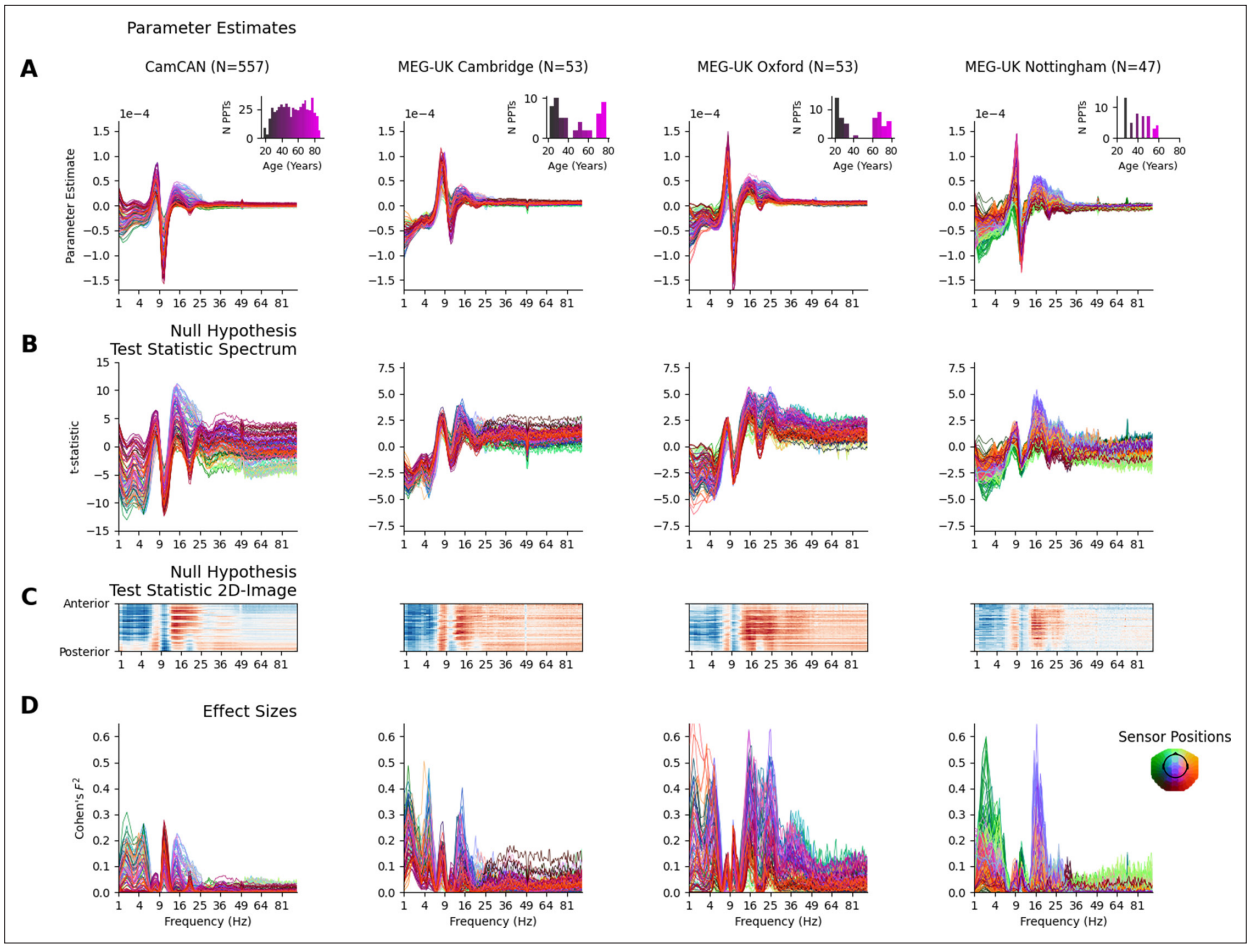


Figure 5. The spatial and spectral profile of the effect of age on resting-state brain electrophysiology is replicable across datasets. (**A**) GLM-Spectrum parameter estimates quantifying the age effect across space and frequency for the four datasets in the replicability analysis with distribution of participant ages shown in the inset figure. The four datasets share the key features highlighted in ***Figure 1***. (**B**) As (A) for t-statistics testing the hypothesis that the parameter estimate of the age effect is different to zero. (**C**) As (B) but visualised as a 2D image in which each row indicates a single sensor with their y-axis position sorted by spatial location on the anterior-posterior axis. (**D**) As (A) for Cohen's F^2 effect sizes for the age regressor in the GLM-Spectrum.

The age effect on the absolute spectrum (***Figure 6***) presents a different pattern of results compared to the relative spectrum (***Figures 1 and 3***). Briefly, the beta effect remains preserved or even enhanced compared to the relative magnitude effect, whilst the alpha effects are attenuated, and the low-frequency effect is decreased or removed altogether (***Figure 6A and B***). There is a reduced spatial specificity in the age effects of absolute power. The largest post hoc cluster of contiguous statistically significance for absolute power covers a broad range of frontal and temporal sensors and stretches the whole 1–95 Hz range of the spectrum (***Figure 6C***) whilst the next four largest clusters have relatively homogenous spatial patterns (***Figure 6C***). Spatial maps are positively correlated for all pairs of frequencies (***Figure 6B***), indicating that absolute scaling from head position might be making a large contribution to the overall effect.

A related decision involves rescaling data recordings to correct for differences in head position within (movement compensation) and between (transformation to reference position) data recordings. This is commonly applied using Signal Space Separation (SSS) with the maxfilter software (***Taulu and Kajola, 2005***; ***Taulu and Simola, 2006***). We additionally compared the age effect across absolute and relative spectral magnitude with three variants of SSS head position correction (none, movement compensation, and movement compensation plus transformation to reference). The spectral profile of the absolute effect (without relative scaling) is relatively consistent across the three variants in SSS head position correction with the application of between recording transformation to reference head

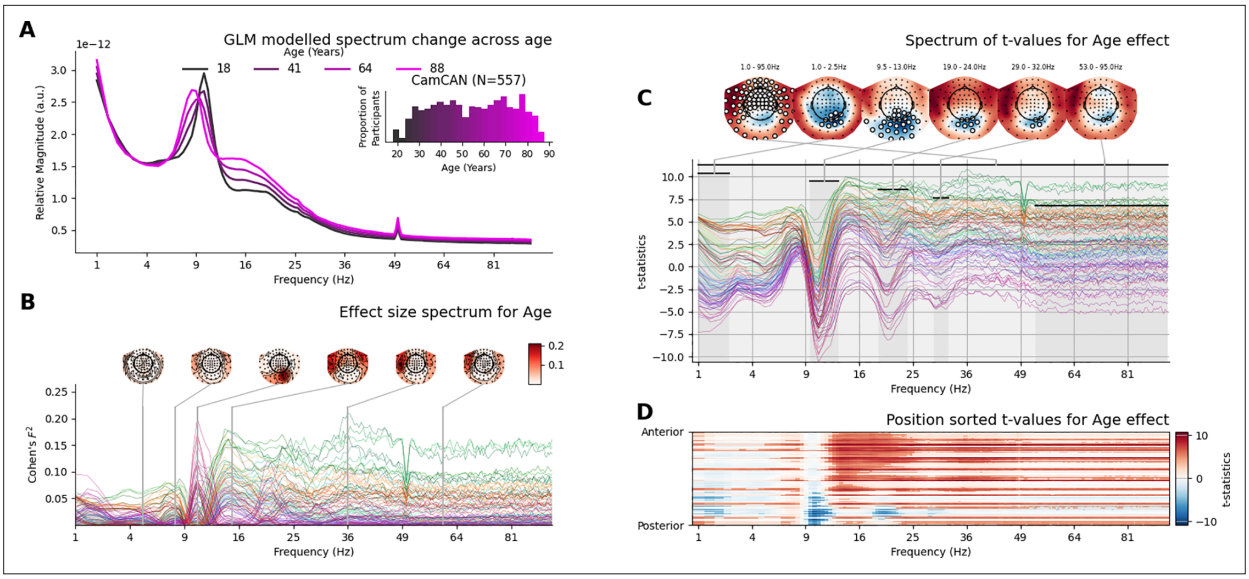


Figure 6. The age effect computed on the absolute magnitude of the power spectrum. (**A**) Model-predicted spectra (averaged across all sensors) for four equally spaced ages across the participant age range with inset histogram of participant ages within Cam-CAN. (**B**) The effect size for the age regressor computed on the absolute magnitude of the power spectrum. (**C**) Top: Spectrum of t-values quantifying the age effect across space and frequency. Non-parametric permutations with maximum statistics to control for multiple comparisons across sensors and frequency bins. While this permutation testing was not cluster-based, contiguous clusters of significant sensors were computed post hoc for visualisation. The largest six spatially and spectrally contiguous areas of statistically significant effects are highlighted in frequency by black bands at the top of the spectrum and highlighted in space by sensors marked with a white circle in the adjoining topography. (**C**) Bottom: A 2D frequency by space map of all statistically significant effects. Sensor-frequency combinations that do not reach statistical significance have a faded colour scale. Blue regions indicate decreasing spectral power with age and red regions indicate increases.

position creating the only noticeable difference (***Appendix 5—figure 2A, C, and E***). In contrast, the relative spectrum has the familiar spectral and spatial profile from ***Figure 1*** and is unaffected by SSS head position correction (***Appendix 5—figure 2B, D, and F***). There is substantially greater spectral specificity in spatial profile of the age effect in relative power, indicated by greater variability in spatial correlations across frequency (***Appendix 5—figure 2G and H***).

Between-participant covariates mediate the age effect differently across the spectrum

Next, we explored whether the age effect is robust when controlling for covariates other than age, i.e., putatively confounding explanatory variables. These alternative covariates may be correlated with age and may impact the estimated relationship between ageing and the observed neuronal power spectrum in complex ways. We selected a non-exhaustive range of alternative covariates split into five categories: demographic (sex), cardiac (heart rate, systolic and diastolic blood pressure), MEG data acquisition (head position in dewar), brain anatomy (brain volume, global grey matter volume [GGMV], global white matter volume, hippocampal volume), and physiological (head radius, height, weight) factors. We do not distinguish between covariates representing neuronally relevant factors and those representing sources of non-neuronal variance.

The GLM-Spectrum was used to quantify the effect of each alternative covariate on the spectrum by fitting a separate GLM for each of the alternative covariates that only contained a regressor for the alternative covariate, alongside an intercept term. Brain volume, GGMV, systolic blood pressure, and sex had the strongest association with the observed MEG power spectrum, though the effect size varies strongly across frequency and space (***Figure 7A*** and Appendix 4).

Next, we compare the age effect in two models: the first includes an age regressor plus intercept, and the second model includes an age regressor, a single alternative covariate regressor, and intercept term. The difference in Cohen's F^2 effect size for age estimated in a simple linear regression model and the partial effect of age from a multiple regression model quantifies how robust the age effect is to the inclusion of the covariate. Including GGMV and systolic blood pressure strongly reduces the

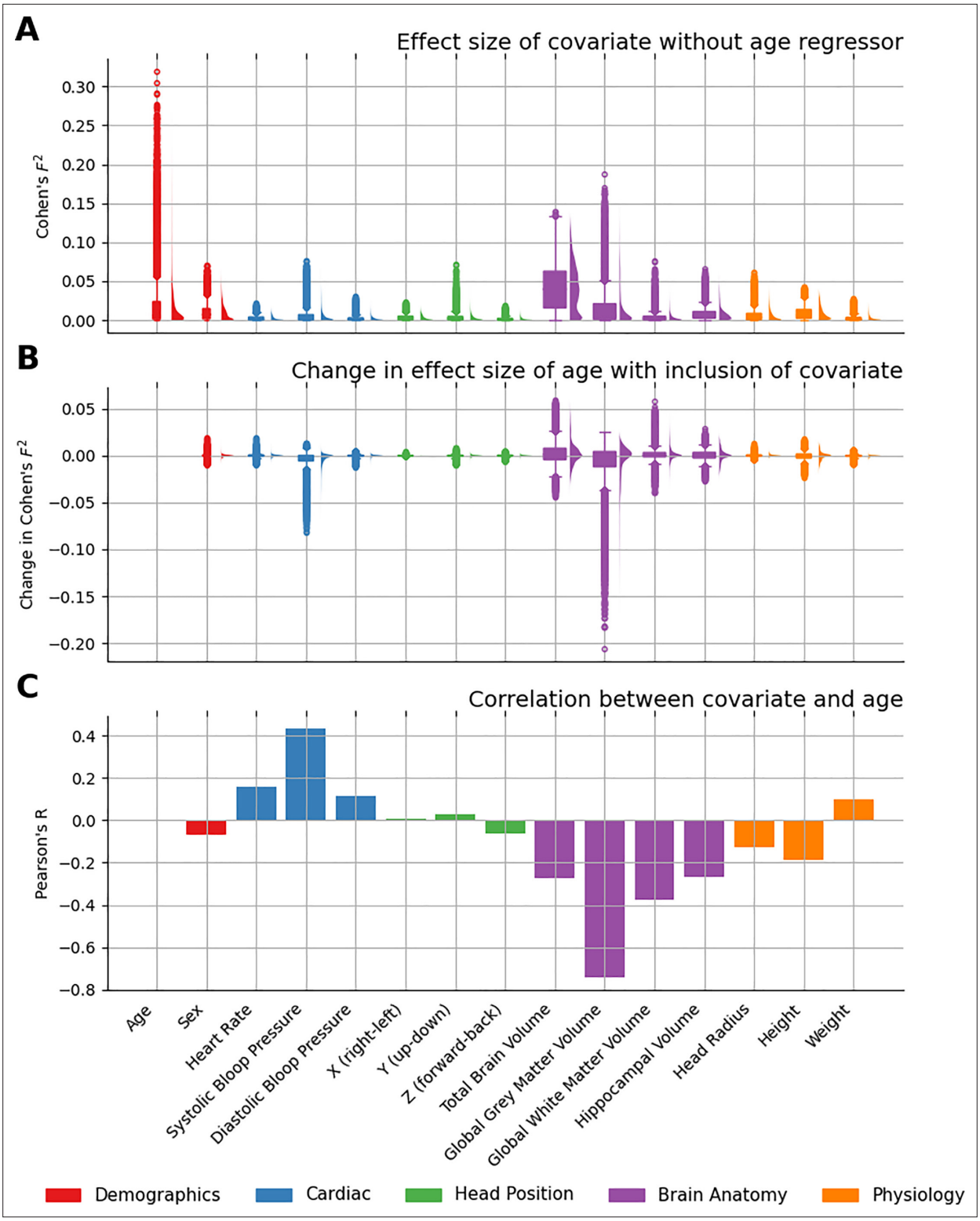


Figure 7. Covariate effect sizes and their impact on the ageing effect. (**A**) Box and whisker plot with paired kernel density plot for the distributions of Cohen's F^2 effect size for each alternative covariate, when the alternative covariate is included as the only regressor in a GLM, along with an intercept term. The Cohen's F^2 distributions are collected over every single sensor-frequency pair from the sensor-space dataset (i.e. over 102 sensors and 189 frequency bins). Full GLM-Spectrum visualisations of the results are included in Appendix 4. For comparison, the same is shown for the age using a GLM that contains regressors for age and an intercept. (**B**) Change in the Cohen's F^2 effect size of age between (1) a GLM that includes an age regressor plus intercept, and (2) a model that includes an age regressor, a single alternative covariate regressor, and intercept. This is shown for each alternative

Figure 7 continued on next page

Figure 7 continued

covariate in turn. Age is excluded from this panel. (**C**) Pearson's correlation coefficient quantifying the univariate linear relationship between age and each covariate. Age and sex are excluded from this panel.

estimated age effect sizes, whilst inclusion of brain volume, white matter volume, or hippocampal volume leads to either increases and decreases in the observed age effect depending on the specific sensor and frequency bin (***Figure 7B*** and ***Appendix 4—figure 4***).

Covariates with low correlation to age (***Figure 7C***) generally did not modify the estimated age effect (e.g. head position, heart rate, and weight). In contrast, including covariates with high correlation can lead to starkly different influences in different brain regions and frequency ranges. For example, including GGMV GG or systolic blood pressure strongly reduced the estimated effect size of age across the brain. In contrast, inclusion of white matter volume or brain volume in the model equally increased and decreased the estimated age effect size, depending on the position and frequency being observed. Systolic blood pressure, white matter volume, and brain volume have comparable correlations with age, but the impact of that correlation on the estimates of the age effect is substantially different.

Isolating the component of the age effect on brain electrophysiology that is distinct from global reduction in grey matter volume

GGMV had the strongest mediating effect on the impact of ageing on the MEG spectrum from all the alternative covariates (***Figure 7***). Whilst there is overlap between age and GGMV in their effect on the MEG spectrum, each has a unique contribution that is distinct from the other. Modelling GGMV alongside age reduced the association between age and neuronal power spectra heterogeneously across different frequency bands and did not reduce the age effect to zero (***Figure 8A and B***).

It is important to note that the correlation between age and GGMV does impact the interpretation of the GLM results, but does not prevent the model fit. We explore the model validation and diagnostics in detail in Appendix 6. In brief, the model is able to separate the unique contribution of age and GGMV. However, the correlation between factors leads to an inflation in the standard error of the estimates. A hypothesis test on these estimates is valid though the inflated variance increases type 2 error by reducing our ability to detect partial effects in the data when they are truly present.

Whilst most of the age effect size spectrum was reduced by inclusion of GGMV, the extent of this reduction varied clearly across the six spatio-spectral regions that showed significant simple linear age effects (see ***Table 2***). Five of the six regions showed a reduction in peak effect size (between –15% and –83%), with a single effect showing a small increase (low gamma range +15%). The regions with the largest initial age effect sizes (before GGMV inclusion) showed the greatest reductions when controlling for GGMV. Despite these reductions, the remaining effect sizes in these regions were still larger than the original effect sizes observed in the regions with initially smaller effects.

These results have a substantial practical impact on study planning. A sample that appears to be well powered for estimating an effect when considering the effect in isolation may in fact be underpowered when covariates and confounds are accounted for in the regression model. Using the present results from Cam-CAN, a study looking to replicate our findings of about the component of the age effect that is linearly distinct from GGMV will require a larger sample than one replicating the age effects alone (***Table 2***). Most critically, two (low alpha and high gamma) of the six identified age effects drop below the significance threshold when accounting for GGMV (***Figure 8***). This suggests that a large part of the electrophysiological effects in these bands cannot be linearly separated from global structural change with ageing.

Discussion

A whole-head and full-frequency profile of the ageing effect is characterised and shown to be replicable across datasets. Six distinct ageing effects are identified, and the combination of linear parameters across the spectrum can represent more complex features such as alpha peak frequency. The corresponding effect sizes demonstrate that age impacts the spectrum heterogeneously and that the feature of interest must be considered when sample size planning for future experiments. This effect is robust to head position correction, but the spatial profile changes substantially between relative

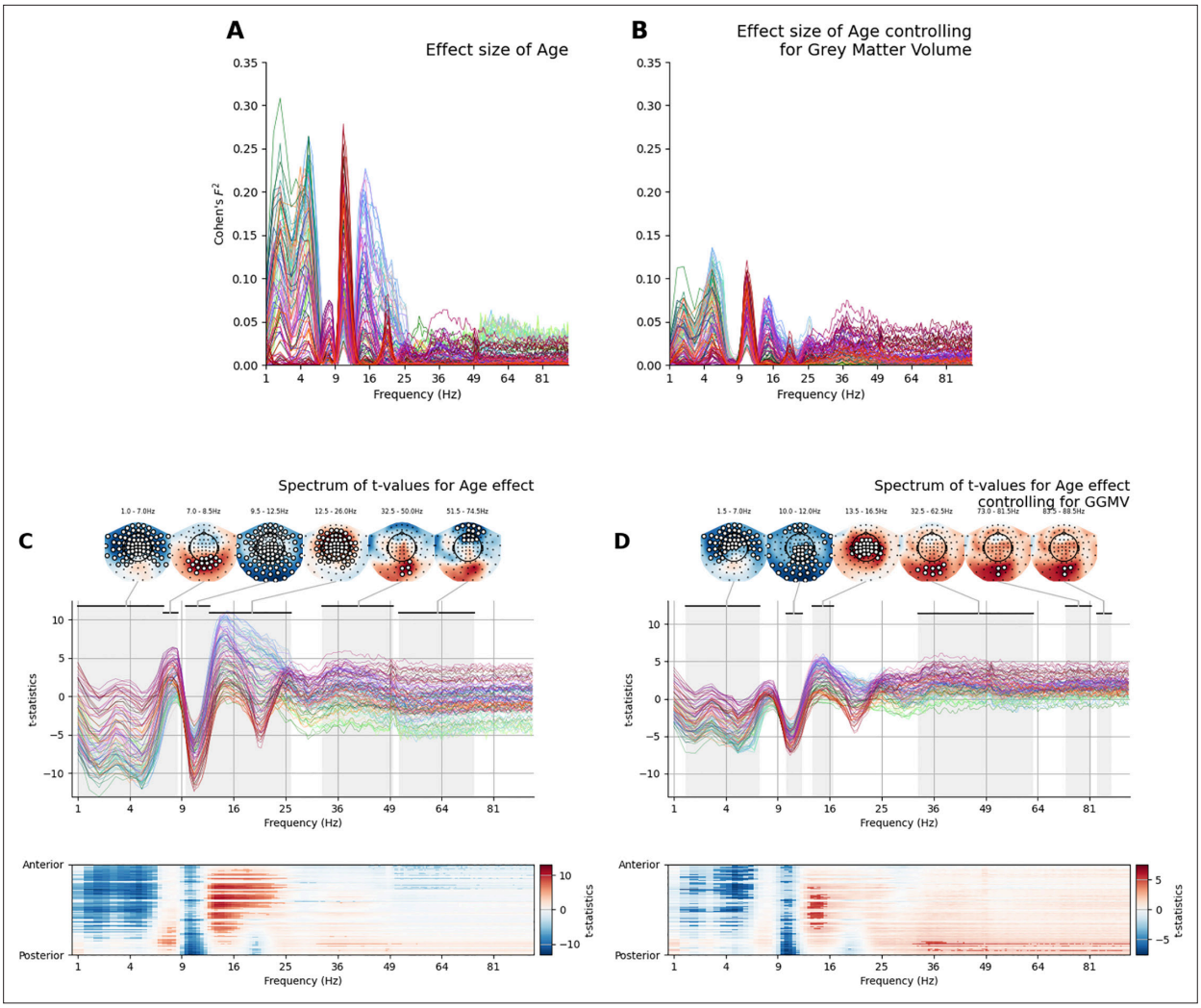


Figure 8. The age effect is reduced heterogeneously across space and frequency by including global grey matter volume (GGMV) in the model. (**A**) The Cohen's F^2 spectrum for age using a GLM that contains regressors for age and an intercept. Replicated from ***Figure 3***. (**B**) As (A) when a grey matter volume regressor is added to the GLM. Accounting for grey matter volume broadly reduces the effect size of age across the spectra, but some moderate effects remain. (**C**) Spectrum of t-values quantifying the age effect across space and frequency replicated from ***Figure 1***. Non-parametric permutations with maximum statistics to control for multiple comparisons across sensors and frequency bins. While this permutation testing was not cluster-based, contiguous clusters of significant sensors were computed post hoc for visualisation. The largest six spatially and spectrally contiguous areas of statistically significant effects are highlighted in frequency by black bands at the top of the spectrum and highlighted in space by sensors marked with a white circle in the adjoining topography. (**D**) As (C) for the age effect in a model that includes a GGMV covariate. Most effects are reduced in size with smaller statistically significant regions surviving the post hoc clustering procedure.

and absolute spectral power. Finally, the age effect is differentially modified by different factors, such as grey matter volume, brain volume, head size, and physiological factors. Individual variability in grey matter volume mediates the association between age and neuronal power spectra, leading to a reduction in the estimated effect size of age across the whole spectrum. Critically, the impact of including a grey matter volume covariate differentially impacts different brain regions and frequency bands, indicating that some regions have a strong and unique signature of ageing that reflects functional/synaptic changes over and above grey matter atrophy.

Overall, by analysing four independent datasets including 710 participants, we demonstrated that there is a replicable and robust effect of ageing on MEG power spectrum across the whole-head and a range of frequencies. These effects are well powered at moderate data samples, replicable across different datasets, and scanner types, and are reasonably robust to modelling additional anatomical, physiological, or acquisition factors as covariates.

Table 2. Summary of significant spatio-spectral regions containing an age effect in Cam-CAN.
The estimated sample sizes are the range of sample sizes needed to have an 80% chance of detecting the effect in a future sample, assuming that both the effects here are true and that the effect sizes are well estimated. Sample size ranges are computed from bootstrapped 95% confidence intervals for effect size estimate. The sample size forecasts are not informative about the present results and serve only as a guide for future study planning.

Analysis and descriptive label	Age effect size	Age effect size with GGMV	Change in age effect size from including GGMV
Effect size estimates			
Low freq (5 Hz)	0.26 (0.19–0.38)	0.11 (0.065–0.18)	–0.15 (–57%)
Low alpha (8 Hz)	0.075 (0.043–0.13)	0.013 (0.0016–0.039)	–0.048 (–83%)
High alpha (10.5 Hz)	0.28 (0.20–0.40)	0.12 (0.080–0.20)	–0.16 (–57%)
Beta (15 Hz)	0.23 (0.16–0.32)	0.078 (0.045–0.13)	–0.152 (–66%)
Low gamma (36 Hz)	0.06 (0.031–0.11)	0.071 (0.034–0.14)	+0.011 (+15%)
High gamma (60 Hz)	0.052 (0.024–0.096)	0.044 (0.015–0.10)	–0.008 (–15%)
	Sample with 80% power for age	Sample with 80% power for age including GGMV	Change in sample for including GGMV
Sample size planning			
Low freq (5 Hz)	25–52	54–148	+30 to +98
Low alpha (8 Hz)	76–225	n.s.	n.s.
High alpha (10.5 Hz)	24–47	49–120	+25 to +73
Beta (15 Hz)	30–60	73–216	+43 to +156
Low gamma (36 Hz)	85–304	67–285	–18 to –19
High gamma (60 Hz)	100–401	n.s.	n.s.

Full-frequency spectra of age effects synthesise diverse results across the literature

The profile of results across the spectrum of age effects replicates and simplifies a range of results across previous literature. This is done without pre-specification of frequency bands or sensors of interest and in a manner that is conducive to future study planning and meta-analyses. Here, we briefly review the core age effects from this analysis in relation to a representative sample of published results on the effects of healthy ageing on the resting-state EEG and MEG spectrum.

Low-frequency power decreases with age

This result is broadly consistent with literature demonstrating that 'theta' power decreases with healthy ageing (***Beese et al., 2017***; ***Cummins and Finnigan, 2007***; ***Rempe et al., 2023***; ***Vlahou et al., 2014***) and may be associated with decreases in cognitive performance (***Finnigan and Robertson, 2011***). One critical difference with this literature is that the full-frequency age profile identifies a single 'low-frequency' age-effect between 1 and 7 Hz and does not distinguish between the canonical delta (2–4 Hz) and theta (4–7 Hz) oscillations. A further difference is that we only see the low-frequency decrease in power in the relative spectrum (***Figure 1***). Computing the age effect from the absolute spectrum resulted in no changes across age at low frequencies (***Figure 6***).

A combination of age-related decreases in lower frequencies with increases in higher frequencies (notably the beta range) contributes to a flattening of the aperiodic component of the power spectrum (***Aggarwal and Ray, 2023***; ***Cesnaite et al., 2023***; ***Dave et al., 2018***; ***Voytek et al., 2015***). This flattening is proposed to reflect an age-related increase in neural noise affecting age-related working memory performance (***Voytek et al., 2015***).

Future research accounting for flattening of the 1/*f*-type component in the full-frequency spectrum approach can better separate whether the low-frequency changes relate to oscillations or the aperiodic component of the spectrum.

Reconciling conflicting reports of the ageing effect on alpha power

The literature exploring how ageing changes alpha power is heterogeneous. Papers that report results in resting alpha power, either from a canonical band or from an individual peak frequency, include reports of a variety of contrasting age effects. This includes positive correlations with age (***Rempe et al., 2023***; ***Stier et al., 2023***), negative correlations (***Thuwal et al., 2021***; ***Lodder and van Putten, 2011***; ***Medrano et al., 2025***; ***Park et al., 2024***), both positive and negative effects separated by space (***Hoshi and Shigihara, 2020***; ***Pathak et al., 2022***), or null results when correcting for individual frequencies and aperiodic slopes (***Scally et al., 2018***; ***Merkin et al., 2023***) (see Appendix 1 for a more detailed summary). There is broad variability in methodological approaches, which could account for the variety of results. ***Stier et al., 2023***, suggest that analyses in sensor or source space may lead to different effects. Critically for our work, this variability also prevents formal aggregation of results and meta-analyses that could clarify the picture.

We have proposed that by taking a step back, and tolerating a reduction in sensitivity, we can map out the whole-head whole-frequency structure of the age effect with minimal researcher degrees of freedom and bias. Investigating age effects as a complete spectrum shows that two contrasting age effects on alpha magnitude coexist in close proximity in space and frequency: an increase with a small effect size in central occipital sensors around 7–8.5 Hz and a decrease with a large effect size across a broad set of occipital, temporal, and frontal sensors between 9.5 and 12.5 Hz. Different data samples and different data analysis choices, particularly the selection of regions of interest, source reconstruction, sensor normalisation, or correction of aperiodic components, might emphasise one effect or the other in each analysis. Whilst we have not conclusively explored all possible variants of these analyses, we have provided a framework that would allow future studies to perform formal comparisons and meta-analyses to resolve this bottleneck.

Relationship between effects on alpha power and alpha individual frequency

The two effects identified in the present analysis may combine to represent a decrease in power and frequency of a single alpha peak (seen qualitatively in ***Figure 1A***). This change in alpha peak frequency is highly replicable (***Cesnaite et al., 2023***; ***Dustman et al., 1993***; ***Sahoo et al., 2020***; ***Scally et al., 2018***; ***Pathak et al., 2022***; ***Zibrandtsen and Kjaer, 2021***) and is a highly predictive spectral marker of ageing (***Stier et al., 2024***). Decreases in alpha peak frequency have been linked to a decline in cognitive performance in healthy ageing (***Cesnaite et al., 2023***; ***Finley et al., 2024***) and MCI (***Garcés et al., 2013***; ***López-Sanz et al., 2016***; ***Puttaert et al., 2021***).

This compelling evidence for a shift in a single peak is complicated by strong evidence for the presence of multiple alpha peaks within individuals (***Quinn et al., 2021***; ***Lodder and van Putten, 2011***; ***Chiang et al., 2011***; ***Chiang et al., 2008***; ***Klimesch, 1999***) with distinct generators and functional relevance (***Sokoliuk et al., 2019***). A complex pattern of changes in power, frequency, and spatial distribution likely underlies age-related change in alpha oscillations. Future work will need to explore all three features at the individual level to clearly illuminate the change.

Linear increase and inverted-U effects in the beta band

The literature reports an increase in low-beta power with age (***Gómez et al., 2013***; ***Heinrichs-Graham and Wilson, 2016***; ***Heinrichs-Graham et al., 2018***; ***Hübner et al., 2018***; ***Koyama et al., 1997***; ***Rempe et al., 2023***; ***Stier et al., 2023***; ***Veldhuizen et al., 1993***; ***Xifra-Porxas et al., 2019***). We have observed inverted-U shaped quadratic effects of age in two frequency ranges in the beta-band, a posterior low-beta component (centred around 18 Hz), and an anterior high-beta component (centred around 25 Hz). This is broadly consistent with reports of quadratic ageing effects in the beta band in the literature (***Gómez et al., 2013***; ***Rempe et al., 2023***; ***Stier et al., 2023***), though to our knowledge, our results are the first to suggest a separation of effects into different parts of the beta range. These spectrum changes may be associated with age-related changes in underlying bursting dynamics (***Brady et al., 2020***; ***Power et al., 2023***).

In addition to changing in the resting state, ageing is associated with increases in movement-related beta desynchronisation (***Bardouille et al., 2019***; ***Heinrichs-Graham and Wilson, 2016***; ***Heinrichs-Graham et al., 2018***; ***Xifra-Porxas et al., 2019***; ***Rossiter et al., 2014***). Changes in post-movement beta rebound have been reported as well (***Bardouille et al., 2019***; ***Xifra-Porxas et al., 2019***). The

increased resting-state beta activity may require increased downregulation in order for older adults to perform movements (***Heinrichs-Graham and Wilson, 2016***).

Novel gamma band changes with age

There are relatively few publications exploring changes in effects of ageing on resting-state gamma band activity. Two EEG studies report increases in gamma power in older adults compared to younger adults (***Aoki et al., 2022***; ***Jabès et al., 2021***). The frequency band of these effects is consistent with our finding though the EEG results indicate a frontoparietal and temporal shift, whereas our gamma increase occurs in occipital sensors. There is larger literature on task related changes in gamma with age, which indicates that gamma responses to visual gratings decrease in power and frequency with age (***Murty et al., 2020***; ***Kumar and Ray, 2023***).

Mediation of age effects by grey matter volume

There are substantial reductions in grey matter volume and cortical thickness across the adult lifespan (***Frangou et al., 2022***). We show that association between age and the resting spectrum is mediated by reductions in grey matter volume, but that this effect is heterogeneous across space and frequency. Our results show that accounting for GGMV reduces the effect sizes of the age effects below 30 Hz by 57–83% (***Figure 8***; ***Table 2***). This reduction replicates results showing that structural brain changes are associated with widespread changes in spectral power (***Stier et al., 2023***). Our results are limited by the use of GGMV as a blunt measure of grey matter change, grey matter decline in ageing occurs heterogeneously across the brain (***Frangou et al., 2022***), and oscillatory changes are likely linked to this pattern (***Mahjoory et al., 2020***).

Observed power analysis for future study planning

The observed power and sample size calculations in this paper should not be used to help interpret the present findings, or as a basis to speculate about what sample size would be required for a non-significant result to pass the significance threshold. Rather they are intended solely to guide decisions about the sample sizes of future studies in an accessible manner and to highlight the potential for this approach in analyses of neuronal power spectra.

We concur with ***Lenth, 2001***, who highlight that 'Sample size planning is often important, and is nearly always difficult'. Most recommendations about sample size planning indicate that a priori or theoretically informed effect sizes should be used as observed effect sizes are influenced by sampling error (***Hoenig and Heisey, 2001***). Single estimates of observed effect sizes can be extremely noisy and will not necessarily reflect the 'true' underlying population effect. Moreover, using the single observed estimate simply recapitulates the information already present in the p-value of the test (***Hoenig and Heisey, 2001***).

As a result, we emphasise the bootstrapped 95% confidence intervals of the effect sizes to give a sense of the uncertainty around our estimates. The upper and lower bound of these confidence intervals are used in the observed power analysis as an example to guide future study planning. Until such a time when the field reaches consensus about what the smallest effect size of interest would be for electrophysiological power spectra, we propose that researchers can use the lower bound of the 95% confidence interval as the smallest effect size of interest for a replication. Working with multiple covariates and a requirement to correct for multiple comparisons both decrease the statistical power of a neuroimaging dataset (***Cremers et al., 2017***) so it is critical to be transparent about which effects are observable in our data. Confidence interval-based sample projections from observed effect sizes must be handled with care but are a useful tool in a field where sample size plans are frequently based on resource constraints or heuristics. Projections can be supported with further sensitivity power analyses that explore a realistic range of expected effect sizes given the context of the planned project. Many excellent guides have been written to inform principled sample size planning in behavioural (***Lakens, 2022***) and neuroimaging contexts (***Mumford, 2012***).

We propose the following steps as a practical guide for researchers looking to plan a data sample with a reasonable chance of correctly identifying a particular effect.

1. **Define research question and identify previous results:** Your research question must be defined in advance and well specified, there should be relevant data or literature that can be used to guide your decision.

2. **Define the smallest effect size of interest and the decision criterion for the sample decision:** It is critical to define the parameters of how you will make your sample size decision ahead of time. We recommend considering what the 'smallest effect size of interest' (***Anvari and Lakens, 2021***) would be for your question. This is specific to your question and is about more than statistical significance. What effect size would indicate that there is a *practically meaningful* effect to for future literature to consider?
3. **Estimate effect sizes to inform your decision:** Either by aggregating reported statistics from the literature or by dedicated processing of previous data, compute an estimate of the effect size. Effect sizes are only estimates so it is important to compute confidence intervals around your estimate to get a measure of variability.
4. **Compute power/precision curves assuming these results:** Using the estimated effect sizes, compute power curves (***Baker et al., 2021***) that visualise the relationship between effect size, statistical power, and sample size.
5. **Select the sample size that meets your pre-defined criteria:** Using your definitions from step 2, and when considering the whole power curve, make a decision about what sample size would give you a reasonable chance of replicating the effect of interest
6. **Make note of any differences or deviations from this plan during your data collection:** There are many practical reasons why your planned sample might not match the data acquired in practice. Such deviations from a plan are ok, but should be acknowledged and any mitigating steps explained (***Lakens, 2024***).
7. **Document your process for inclusion in a preregistration or publication:** Include details on how a sample size decision was made in your research outputs, including preregistrations, preprints, and publications. These details will be useful for future researchers to understand your process and to implement their own.

Limitations

Our approach promotes an exploratory and unbiased approach to quantifying the age effect on neuronal power spectra, which is intended to complement more focused analyses. This has the benefit of reducing researcher's degrees of freedom and of being broadly generalisable. These come at the cost of a loss in specificity and in sensitivity. Our approach does not specifically quantify features derived from the power spectrum such as alpha-peak frequency or the aperiodic component of the spectrum. These features are mixed into our full spectrum estimates but not directly quantified. Thus, they can be challenging to interpret from our approach. Secondly, the mass-univariate approach suffers from a potential loss in sensitivity compared to results that aggregate across spatial or spectral regions that contain consistent results. Where a region or frequency band of interest can be supported from the literature, an approach focusing on a single region has the benefit of reduced noise by averaging estimates from a larger range of observations. Finally, models that consider the whole shape of the spectrum (***Donoghue et al., 2021***) would also be able to combine information across a range of frequencies rather than depending on a single frequency bin for each estimate. These models have the additional benefit that their parameters are often directly interpretable as features of interest, such as spectral slope or peak frequency.

Whilst we have explored the impact of several analysis decisions on the profile of the ageing effect, we have not completed an exhaustive search of the processing options available to electrophysiology researchers. We have demonstrated that the age effect is robust to SSS-based head position correction and to a broad range of covariates but modified by choice of relative or absolute power and inclusion of grey matter volume as a covariate. A broad range of analysis options are still to be explored, notably including the impact of different source reconstruction methods beyond the single example presented here. This is not an exhaustive exploration of the garden of forking paths (***Gelman and Loken, 2013***), and future analysis can broaden this scope through approaches such as multiverse analysis methods (***Clayson et al., 2021***; ***Dafflon et al., 2022***).

Both absolute and relative power measures are used throughout the literature, but there is little consensus about their interpretation (***Sandre and Troller-Renfree, 2026***). We focus on relative power for most of our results. By normalising each participant's power spectrum by the sum across frequencies, we found that the results gained specificity in frequency band and reduced concern about wide inter-subject differences in overall variance. Though this improved some analyses, relative power has important drawbacks. In particular, it can reduce sensitivity to effects that are broadly distributed across the spectrum and uses arbitrary scaling rather than meaningful physical units. We support calls

in the literature to report both relative and absolute power measures (***Rempe et al., 2023***; ***Sandre and Troller-Renfree, 2026***) as they contain complementary insights.

We have compiled results from a broad range of whole-head and full-frequency models to provide a comprehensive overview of the linear age effect. However, due to the complexity of the data, further analysis is still needed to explore various options. We have only explored the linear effects of age in these analyses, whilst there is evidence for quadratic age effects in power spectral features (***Brady et al., 2020***; ***Rempe et al., 2023***). Our current analysis pipeline may not adequately capture variability in individual data recordings by neglecting to incorporate first-level variance components into the group model. A mixed modelling approach would provide a more comprehensive and robust framework for analysing these data. Finally, we present results based on spectral magnitude rather than power or log-power as a compromise between suitability for Gaussian linear modelling and intuitive presentation of findings (***Quinn et al., 2024***).

Building towards robust and reproducible effects of age in brain electrophysiology

We propose that computing and sharing unthresholded whole-head and full-frequency statistical spectra of key effects can facilitate comparability between studies. In addition, the spectra of ageing effect sizes can support formal meta-analyses and planning of future sample sizes. We propose that this simple approach can provide a robust and replicable foundation stone on which clinical applications and more advanced analysis methodologies can be built and validated.

Similar approaches have been successful in facilitating the synthesis and crosstalk of results across a diverse literature in MRI (***Gorgolewski et al., 2015***). To date, meta-analyses of spectral effects of ageing have been limited to features within specified frequency bands, such as alpha band peak frequency (***Freschl et al., 2022***) or power (***Lejko et al., 2020***). These analyses are currently limited by variable and often incomplete reporting of results in addition to cumbersome decisions about how to combine results across heterogeneous channel sets, spatial regions, and frequency bands. Best practice reporting guidelines (***Gross et al., 2013***) and formal reporting standards, such as COBIDAS-MEEG (***Pernet et al., 2018***), improve transparency, but there is still a need to share outputs in a form that can readily support synthesis across studies and establish consensus about core effects.

Future extensions

A clear future extension for this work is to formally incorporate estimates of within-subject variability into a mixed-effect model. These powerful models would enable modelling of both fixed effects and random effects, allowing researchers to account for variation within individuals over time and between individuals. Linear mixed models also provide improved approaches for handling missing observations and unbalanced designs, making them especially useful for longitudinal and hierarchical data. A second expansion of this work could use generalised additive mixed models to model non-linear relationships using smooth functions while also accounting for random effects. This may allow for more realistic representations of complex patterns of change across age. Linear mixed modelling comes with a substantial increase in researcher degrees of freedom and can be challenging to implement and report accurately (***Meteyard and Davies, 2020***). We have used fixed-effects modelling in this work in line with our objectives of maintaining generalisability and minimising researcher degrees of freedom.

Conclusion

Overall, we have demonstrated that ageing effects on MEG power spectra are robust and replicable across multiple datasets. Different brain regions and frequency bands respond differently to ageing, with some having a strong unique signature of ageing that is dissociable from global anatomical changes. This is a necessary step towards adoption of electrophysiological measures in a healthcare setting.

Methods

Datasets

Four open-access cross-sectional datasets with participants covering a broad age range were analysed as part of this manuscript.

Cam-CAN

Data used in the preparation of this work were obtained from the Cam-CAN repository (*N*=571, 284 female, mean age = 54 years of age, age range = 18–88 years of age), available at http://www.mrc-cbu.cam.ac.uk/datasets/camcan/, ***Taylor et al., 2017***; ***Shafto et al., 2014***. The Cam-CAN study was conducted in compliance with the Helsinki Declaration and has been approved by the local ethics committee, Cambridgeshire 2 Research Ethics Committee (reference: 10/H0308/50).

MEG-UK Oxford, Cambridge, and Nottingham

Eyes closed resting-state MEG recordings were acquired in three MEG laboratories in the United Kingdom as part of the wider MEG-UK consortium: Oxford (*N*=80, 38 female, mean age = 48 years of age, age range = 20–80 years of age), Cambridge (*N*=80, 39 female, mean age = 47, age range = 21–78 years of age), and Nottingham (*N*=74, 39 females, mean age = 39 years of age, age range = 27–60 years of age). The Oxford and Cambridge data was acquired on a 306-channel VectorView system whilst the Cardiff and Nottingham data was acquired on a CTF-275 channel system. The MEGUK study was conducted in compliance with the Helsinki Declaration, with approval from local ethics committees at each host site.

MEG data pre-processing

All MEG data pre-processing was carried out using MNE-Python (***Gramfort et al., 2013***) and OSL-ephys (***Quinn et al., 2022***; ***van Es et al., 2025***) using the OSL batch pre-processing tools. For the Cam-CAN data, we proceeded with analysis on post-maxfilter processed data provided by the Cam-CAN team. Briefly, the data were processed using AA (***Cusack et al., 2014***) with automatic bad channel detection (limited to seven channels) with the origin set to the centre of a sphere fitted to the individual's Polhemus headshape points. Maxfilter signal-space separation was performed with the temporal extension enabled (temporal window of 10 s and correlation threshold of $r = 0.98$). Head position was continuously estimated and compensated for during periods where the HPI coils were on. After maxfilter processing, head positions were translated into a default head position defined as a point relative to each individual's origin in a head coordinate frame. Data with the full maxfilter processing and with the head position translation or movement compensation were extracted from the Cam-CAN database. An equivalent pipeline was implemented in OSL-Ephys and applied to the data from the MEG-UK datasets from Oxford and Cambridge. Files from the MEG-UK Nottingham dataset were processed with third-order gradiometry applied.

The data from each recording was first converted from its raw format into MNE-Python Raw data objects. The first 35 s of continuous data were cropped out, and the remaining data were bandpass filtered between 0.25 and 150 Hz using an order 5 Butterworth filter. 50 Hz line noise was suppressed using the ZapLine method (***de Cheveigné, 2020***) as implemented in the MEEGKit toolbox. Two passes of ZapLine were applied to account for minor peaks around the 50 Hz artefact. One pass was centred on 49 Hz and the second on 50 Hz. Bad segments were identified by segmenting data into 2 s chunks and using the generalised-extreme studentized deviate (***Rosner, 1983***) algorithm to identify outlier (bad) samples with high variance across channels. Bad segment detection was applied to both the raw time series and the differential of the time series and separately to the magnetometers and gradiometers. An average of 2.82% of data samples were marked as 'bad' (standard deviation: 2.54%, min: 0.0%, max: 15.52%) equivalent to an average of 15.04 s per recording. Bad channels were then identified using the G-ESD routine to identify outliers in the distribution of variance per channel over time. The data were then resampled to 250 Hz to reduce space on-disk and ease subsequent computations.

Independent component analysis (ICA) denoising was carried out using a 64-component FastICA decomposition (***Hyvärinen, 1999***) on the MEG channels. This decomposition explained an average of 99% of variance in the sensor data across datasets. Artefactual components relating to eye movements or the heart rate were automatically identified by correlation with the simultaneous EOG and ECG channels. ECG artefacts were identified using cross-trial phase statistics (***Dammers et al., 2008***) and an automatic threshold based on the sample rate of the data as implemented in the `mne.preprocessing.ICA.find bads ecg` function in MNE Python. Between 0 and 3 EOG components were rejected in each dataset, with an average of 0.99 (standard deviation: 0.79) across all datasets. EOG artefacts were identified by correlation with the HEOG and VEOG channels with a threshold set to $r = 0.35$ as implemented in the `mne.preprocessing.ICA.find bads eog` function in MNE Python.

Between 0 and 5 ECG components were rejected in each dataset, with an average of 2.25 (standard deviation: 0.84) across all datasets. The continuous sensor data were then reconstructed without the influence of the components labelled as artefacts. A total of 557 participants had all data present and completed pre-processing from the Cam-CAN dataset.

To retain consistent dimensionality across the group, any bad channels were interpolated using a spherical spline interpolation (***Perrin et al., 1989***) as implemented in MNE-Python. The head position of the participant in device coordinates was extracted from each dataset.

This pipeline was repeated for both the SSS-processed data with and without movement compensation and head position standardisation.

The same pipeline was applied to the VectorView data from the Oxford and Cambridge sites of the MEGUK dataset. A very similar pipeline was applied to the CTF data from the Nottingham site of the MEGUK dataset, except for omitting the SSS processing in favour of third-order gradiometry and in selection of planar gradiometer channels. A total of 53 participants for Oxford and Cambridge, and 47 participants had all data present and completed pre-processing for the MEGUK dataset.

MRI data processing

All MR data were processed using the FMRIB Software Library (***Woolrich et al., 2009***). T1-weighted MR scans from 804 individuals were analysed. Images were reoriented to MNI space, cropped, and bias-field corrected. FMRIB's Linear Registration Tool, FLIRT (***Jenkinson and Smith, 2001***; ***Jenkinson et al., 2002***), was used to register to standard space before brain extraction was performed using BET (***Smith, 2002***). Tissue-type segmentation (grey matter, white matter, and CSF) was conducted using FMRIB's Automated Segmentation Tool, FAST (***Zhang et al., 2001***). Subcortical structure volumes (hippocampus, amygdala, etc.) were derived using FMRIB's Integrated Registration and Segmentation Tool (***Patenaude et al., 2011***).

Total head volume was computed by extracting a volumetric skull mask using the FSL BETSurf tool and filling in the gap left by brain extraction. The total number of voxels within the head and brain was computed with fslmaths. The overall brain volume was normalised by the total head volume.

The voxel count for each tissue-type and subcortical structure was extracted and normalised using the individual's total brain volume (computed by FAST) to compute a percentage. The final MRI metrics were: total head volume, brain volume (as a proportion of head volume), GGMV (grey matter volume as a proportion of total brain volume), and hippocampus volume (summed across left and right hemispheres as a proportion of total brain volume).

Source reconstruction and parcellation

First, a structural MRI (sMRI) was used to coregister the MEG data. This involved extracting surfaces for the outer skin, outer skull, and inner skull from the sMRI using FSL, then aligning the Polhemus headshape points to the outer skin surface, as well as aligning the sMRI and Polhemus fiducials. Note, 31 out of 643 subjects from Cam-CAN were excluded at this stage due to missing sMRIs.

Following the coregistration, a single-shell forward model was computed. The pre-processed sensor-level data were source-reconstructed using a linearly constrained minimum variance (LCMV) beamformer (***Hillebrand et al., 2005***; ***Van Veen and Buckley, 1988***). This involved projecting the sensor-level data onto an 8 mm dipole grid inside the inner skull. The forward model and sensor-level data covariance matrix were used to compute the LCMV beamformer. The covariance matrix was estimated using the entire recording for a subject and regularised to 60 components using principal component analysis rank reduction.

Using the dipole time courses from source reconstruction, parcel time courses were calculated using an anatomical parcellation with 52 regions of interest (binary) (***Kohl et al., 2023***). The first principal component across dipoles assigned to a parcel was used to generate the parcel time courses. Following this, the parcel time courses were orthogonalised using a symmetric multivariate correction for spatial leakage (***Colclough et al., 2015***). Finally, a stochastic search algorithm was used to align the sign of each parcel time course across subjects by matching to a (median) template subject.

GLM-Spectrum – first level

A GLM-Spectrum (***Quinn et al., 2024***) was used to provide a statistical estimate of the MEG spectrum in the presence of covariates and confounds. A short-time Fourier transform (STFT) was computed

from the pre-processed sensor time series from each dataset using a 2 s segment length, a 1 s overlap between segments, and a Hanning taper. The 2 s segment length at the sample rate of 250 Hz gives a resolution of around 2 frequency bins per unit Hertz in the resulting spectrum. The short-time magnitude spectrum is computed from the complex-valued STFT and the frequency bins ranging between 0.1 and 100 Hz taken forward as the dependent variable in the first-level GLM-Spectrum for that dataset.

The GLM design matrix for each dataset is specified with five regressors. A single constant regressor models the intercept of the data, whilst two zero-mean parametric regressors model the effect of changing heart rate and a linear trend in time throughout the recording. The fourth and fifth regressors were non-zero mean parametric regressors modelling the effect of variance in the V-EOG channel and bad segments. These final regressors acted as confound variables that removed variance that can be linearly explained by the artefact sources from the mean term.

A set of simple contrasts isolated the main effect of each of the five regressors. The first-level GLM-Spectrum model parameters were estimated using the Moore-Penrose pseudo-inverse (***Penrose, 1956***) to compute beta-spectra. Finally, the beta-spectra were weighted by the contrasts to compute cope-spectra, which were carried forward to the group-level analyses.

GLM-Spectrum – group-level effect of age

A group-level design matrix was constructed with two regressors, one constant intercept term and one parametric regressor containing z-standardised participant age. The input data were the first-level average magnitude spectrum from each participant. The model coefficients were computed using the Moore-Penrose pseudo-inverse before contrasts and t-statistics were computed. Non-parametric permutation statistics were used to compute the statistical significance by row-shuffling the age regressor. Multiple comparisons were controlled by taking a maximum-statistic across all sensors and frequency bins. Contiguous clusters of significant effects were identified to simplify the final visualisation of the results. Cohen's F^2 was computed for the age regressor for all sensors and frequency bins.

A second group-level design matrix was constructed to explore quadratic effects of age. This design contained three regressors, the intercept, a z-standardised age regressor, and a z-standardised age regressor raised to a power of 2 to quantify quadratic components. The model fit, validation, and statistical assessment of the quadratic predictor of this model were performed in the same way as the linear effect in the previous model.

GLM-Spectrum – group-level effect between subject covariates

Eleven potential between-subject covariates were collated for group analysis and are summarised in ***Table 2***. To explore the individual effect of each covariate, a separate two-regressor model containing a constant term and a covariate was fitted for each covariate in turn. Non-parametric permutation statistics were used to estimate statistical significance for each of the covariates in these simple models. The effect size of each covariate in the simple models was computed using Cohen's F^2 statistics.

Single regressor models

The core model contained two regressors, one constant term and one z-transformed age regressor. This model was computed twice on different pre-processing versions of the Cam-CAN dataset, once using the full first-level GLM-Spectra and once without the additional covariates (linear trend, EOG, ECG, and bad segments) in the first level.

Age plus quadratic age models

To move beyond linear change and explore U and inverted-U shaped effects of age, we fitted a group model with three regressors. One constant term, one z-transformed age regressor, and one z-transformed quadratic age regressor $(age - mean(age))^2$.

Age plus covariate models

The effect of each covariate on the overall effect of age was explored by fitting a second set of models that contain a constant term, the age covariate, and each individual other covariate in turn. Statistical significances and effect sizes were computed for the age effect in each individual model. The change

in effect size of the age covariate between the single regressor age model and the age-plus-covariate models was computed for each covariate.

Effect size and power analyses

Effect sizes are computed using Cohen's F^2 metric, which compares the R^2 of two models to establish the contribution of a particular regressor to the variance explained by the model (***Cohen, 1988***; ***Selya et al., 2012***). Cohen's F^2 can be interpreted as the proportion of residual variance explained by the addition of the new regressor.

The effect size is defined as:

$$Cohen'sF^2 = \frac{R^2_{AB} - R^2_A}{1 - R^2_{AB}} \quad (1)$$

where *B* refers to the regressor of interest and *A* refers to the set of all other regressors in the model. The numerator is then the proportion of additional variance explained by the addition of the regressor of interest *B*. This is normalised by the denominator, which quantifies the total residual variance left unexplained by the full model (***Selya et al., 2012***). A full spectrum of effect sizes can be computed from the GLM-Spectrum model (***Quinn et al., 2024***).

Bootstrapped confidence intervals for effect size estimates were computed by building a distribution of effect sizes using 1000 iterations of resampling with replacement. 95% confidence intervals were computed as percentiles across the bootstrapped distribution of effect size estimates. Confidence intervals for power and sample size calculations are computed using the bootstrapped Cohen's F^2 metrics.

Power analysis for regressors in a general linear model was computed using in-house Python code validated against the pwr R package (***Champely, 2020***; ***Cohen, 1988***). Five variables were defined, of which any four can be used to compute the remaining fifth variable. For a GLM, these variables are the number of observations in the data, the number of regressors in the model, the estimated effect size, the alpha level (type 1 error), and the power (1 – type 2 error). We computed the future sample size estimates in ***Tables 1 and 2*** using this approach. The number of observations in the dataset was computed from the number of regressors in the model (2 or 3), the Cohen's F^2 estimate, an alpha level of 0.05, and a power of 80%.

Acknowledgements

This research was supported by the National Institute for Health Research (NIHR) Oxford Health Biomedical Research Centre. The Wellcome Centre for Integrative Neuroimaging is supported by core funding from the Wellcome Trust (203139/Z/16/Z). CG is supported by the Wellcome Trust (215573/Z/19/Z). OK is supported by the Marie Sklodowska-Curie Innovative Training Network 'European School of Network Neuroscience (euSNN)' (860563). MWJvE is supported by the Wellcome Trust (106183/Z/14/Z, 215573/Z/19/Z), the New Therapeutics in Alzheimer's Diseases (NTAD) supported by the MRC and the Dementia Platform UK (RG94383/RG89702). ACN is supported by the Wellcome Trust (104571/Z/14/Z) and James S McDonnell Foundation (220020448). MWW is supported by the Wellcome Trust (106183/Z/14/Z, 215573/Z/19/Z), the New Therapeutics in Alzheimer's Diseases (NTAD) study supported by UK MRC, the Dementia Platform UK (RG94383/RG89702), and the NIHR Oxford Health Biomedical Research Centre (NIHR203316). The views expressed are those of the author(s) and not necessarily those of the NIHR or the Department of Health and Social Care.

For the purpose of open access, the author has applied a CC-BY public copyright licence to any Author Accepted Manuscript version arising from this submission.

The computations described in this paper were performed using the University of Birmingham's BlueBEAR HPC service, which provides a High Performance Computing service to the University's research community. See http://www.birmingham.ac.uk/bear for more details.

Additional information

Funding

Funder	Grant reference number	Author
Wellcome Trust	203139/Z/16/Z	Anna C Nobre Mark W Woolrich
Wellcome Trust	215573/Z/19/Z	Chetan Gohil Mats WJ van Es Anna C Nobre Mark W Woolrich
Marie Curie	860563	Oliver Kohl
Wellcome Trust	106183/Z/14/Z	Mats WJ van Es Anna C Nobre Mark W Woolrich
Medical Research Council	RG94383	Andrew J Quinn Anna C Nobre Mark W Woolrich
Medical Research Council	RG89702	Andrew J Quinn Anna C Nobre Mark W Woolrich
NIHR Oxford Biomedical Research Centre	NIHR203316	Anna C Nobre Mark W Woolrich
Wellcome Trust	104571/Z/14/Z	Anna C Nobre

The funders had no role in study design, data collection and interpretation, or the decision to submit the work for publication. For the purpose of Open Access, the authors have applied a CC BY public copyright license to any Author Accepted Manuscript version arising from this submission.

Author contributions

Andrew J Quinn, Conceptualization, Data curation, Software, Formal analysis, Visualization, Methodology, Writing – original draft, Project administration, Writing – review and editing; Jemma Pitt, Conceptualization, Data curation, Formal analysis, Methodology, Writing – review and editing; Oliver Kohl, Conceptualization, Writing – original draft, Writing – review and editing; Chetan Gohil, Conceptualization, Data curation, Software, Formal analysis, Methodology, Writing – review and editing; Mats WJ van Es, Conceptualization, Writing – review and editing; Anna C Nobre, Conceptualization, Supervision, Writing – review and editing; Mark W Woolrich, Conceptualization, Supervision, Methodology, Writing – original draft, Writing – review and editing

Author ORCIDs

Andrew J Quinn https://orcid.org/0000-0003-2267-9897
Jemma Pitt https://orcid.org/0000-0001-6256-6091
Oliver Kohl https://orcid.org/0000-0003-3166-8145
Chetan Gohil https://orcid.org/0000-0002-0888-1207
Mats WJ van Es https://orcid.org/0000-0002-7133-509X
Anna C Nobre https://orcid.org/0000-0001-5762-2802
Mark W Woolrich https://orcid.org/0000-0001-8460-8854

Ethics

This study did not directly recruit, consent or test human participants, it involves analysis of secondary datasets that were made available after the original authors collected collected data in compliance with the Helsinki Declaration, and with approval by their respective local ethics committees.

Peer review material

Version of Record:
Reviewer #1 (Public review): https://doi.org/10.7554/eLife.108829.3.sa1
Reviewer #2 (Public review): https://doi.org/10.7554/eLife.108829.3.sa2
Author response https://doi.org/10.7554/eLife.108829.3.sa3

Reviewed preprint v2
Reviewer #1 (Public review): https://doi.org/10.7554/eLife.108829.2.sa2
Reviewer #2 (Public review): https://doi.org/10.7554/eLife.108829.2.sa1
Author response: https://doi.org/10.7554/eLife.108829.2.sa0
eLife Assessment https://doi.org/10.7554/eLife.108829.2.sa3

Reviewed preprint v1
Reviewer #1 (Public review): https://doi.org/10.7554/eLife.108829.1.sa1
Reviewer #2 (Public review): https://doi.org/10.7554/eLife.108829.1.sa0
eLife Assessment https://doi.org/10.7554/eLife.108829.1.sa2

Additional files

Supplementary files

MDAR checklist

Data availability

Raw sensor-level MEG recordings are from the CamCAN Data Repository: https://opendata.mrc-cbu.cam.ac.uk/projects/camcan/ (Eyes Closed Resting State data) and the MEG-UK Database https://meguk.ac.uk/database/ (Eyes closed resting data from Oxford, Cambridge & Nottingham). Preprocessed and analysed data to reproduce group level analyses are archived on the Open Science Framework : https://osf.io/yspdg/. Code to run all processing, data analysis and visualisations are available on github (GitHub: https://github.com/OHBA-analysis/Quinn2025-RobustReplicableAge copy archived at ***Quinn, 2025***). The analyses in this paper were carried out in Python 3.11 with core dependencies as numpy (***Harris et al., 2020***), scipy (***Virtanen et al., 2020***) and Matplotlib (***Hunter, 2007***). MNE python (***Gramfort et al., 2013***) was used for EEG/MEG data processing with OSL batch processing tools (***Quinn et al., 2022***; ***van Es et al., 2025***). The spectrum analyses further depend on the Spectrum Analysis in Linear Systems toolbox (***Quinn and Hymers, 2020***) and glmtools (https://pypi.org/project/glmtools/).

The following dataset was generated:

Author(s)	Year	Dataset title	Dataset URL	Database and Identifier
Quinn A, Pitt J, Kohl O, Gohil C, Nobre AC, Woolrich M, van Es MWJ	2025	Robust and replicable effects of ageing on resting state brain electrophysiology measured with MEG	https://osf.io/yspdg/	Open Science Framework, yspdg

References

Aggarwal S, Ray S. 2023. Slope of the power spectral density flattens at low frequencies (200 Hz) in human electroencephalogram. *Cerebral Cortex Communications* **4**:tgad011. DOI: https://doi.org/10.1093/texcom/tgad011, PMID: 37334259

Anvari F, Lakens D. 2021. Using anchor-based methods to determine the smallest effect size of interest. *Journal of Experimental Social Psychology* **96**:104159. DOI: https://doi.org/10.1016/j.jesp.2021.104159

Aoki Y, Hata M, Iwase M, Ishii R, Pascual-Marqui RD, Yanagisawa T, Kishima H, Ikeda M. 2022. Cortical electrical activity changes in healthy aging using EEG-eLORETA analysis. *Neuroimage. Reports* **2**:100143. DOI: https://doi.org/10.1016/j.ynirp.2022.100143, PMID: 40567558

Babiloni C, Binetti G, Cassarino A, Dal Forno G, Del Percio C, Ferreri F, Ferri R, Frisoni G, Galderisi S, Hirata K, Lanuzza B, Miniussi C, Mucci A, Nobili F, Rodriguez G, Luca Romani G, Rossini PM. 2006. Sources of cortical rhythms in adults during physiological aging: a multicentric EEG study. *Human Brain Mapping* **27**:162–172. DOI: https://doi.org/10.1002/hbm.20175, PMID: 16108018

Babiloni C, Blinowska K, Bonanni L, Cichocki A, De Haan W, Del Percio C, Dubois B, Escudero J, Fernández A, Frisoni G, Guntekin B, Hajos M, Hampel H, Ifeachor E, Kilborn K, Kumar S, Johnsen K, Johannsson M, Jeong J, LeBeau F, et al. 2020. What electrophysiology tells us about Alzheimer's disease: a window into the synchronization and connectivity of brain neurons. *Neurobiology of Aging* **85**:58–73. DOI: https://doi.org/10.1016/j.neurobiolaging.2019.09.008, PMID: 31739167

Baker DH, Vilidaite G, Lygo FA, Smith AK, Flack TR, Gouws AD, Andrews TJ. 2021. Power contours: Optimising sample size and precision in experimental psychology and human neuroscience. *Psychological Methods* **26**:295–314. DOI: https://doi.org/10.1037/met0000337, PMID: 32673043

Bardouille T, Bailey L, CamCAN Group. 2019. Evidence for age-related changes in sensorimotor neuromagnetic responses during cued button pressing in a large open-access dataset. *NeuroImage* **193**:25–34. DOI: https://doi.org/10.1016/j.neuroimage.2019.02.065, PMID: 30849530

Beese C, Meyer L, Vassileiou B, Friederici AD. 2017. Temporally and spatially distinct theta oscillations dissociate a language-specific from a domain-general processing mechanism across the age trajectory. *Scientific Reports* **7**:11202. DOI: https://doi.org/10.1038/s41598-017-11632-z, PMID: 28894235

Botvinik-Nezer R, Wager TD. 2023. Reproducibility in neuroimaging analysis: challenges and solutions. *Biological Psychiatry. Cognitive Neuroscience and Neuroimaging* **8**:780–788. DOI: https://doi.org/10.1016/j.bpsc.2022.12.006, PMID: 36906444

Brady B, Power L, Bardouille T. 2020. Age-related trends in neuromagnetic transient beta burst characteristics during a sensorimotor task and rest in the Cam-CAN open-access dataset. *NeuroImage* **222**:117245. DOI: https://doi.org/10.1016/j.neuroimage.2020.117245, PMID: 32818620

Button KS, Ioannidis JPA, Mokrysz C, Nosek BA, Flint J, Robinson ESJ, Munafò MR. 2013. Power failure: why small sample size undermines the reliability of neuroscience. *Nature Reviews. Neuroscience* **14**:365–376. DOI: https://doi.org/10.1038/nrn3475, PMID: 23571845

Cesnaite E, Steinfath P, Jamshidi Idaji M, Stephani T, Kumral D, Haufe S, Sander C, Hensch T, Hegerl U, Riedel-Heller S, Röhr S, Schroeter ML, Witte AV, Villringer A, Nikulin VV. 2023. Alterations in rhythmic and non-rhythmic resting-state EEG activity and their link to cognition in older age. *NeuroImage* **268**:119810. DOI: https://doi.org/10.1016/j.neuroimage.2022.119810, PMID: 36587708

Champely S. 2020. Pwr: basic functions for power analysis. CRAN Package. https://CRAN.R-project.org/package=pwr

Chiang AKI, Rennie CJ, Robinson PA, Roberts JA, Rigozzi MK, Whitehouse RW, Hamilton RJ, Gordon E. 2008. Automated characterization of multiple alpha peaks in multi-site electroencephalograms. *Journal of Neuroscience Methods* **168**:396–411. DOI: https://doi.org/10.1016/j.jneumeth.2007.11.001, PMID: 18083237

Chiang AKI, Rennie CJ, Robinson PA, van Albada SJ, Kerr CC. 2011. Age trends and sex differences of alpha rhythms including split alpha peaks. *Clinical Neurophysiology* **122**:1505–1517. DOI: https://doi.org/10.1016/j.clinph.2011.01.040, PMID: 21349761

Clayson PE, Baldwin SA, Rocha HA, Larson MJ. 2021. The data-processing multiverse of event-related potentials (ERPs): A roadmap for the optimization and standardization of ERP processing and reduction pipelines. *NeuroImage* **245**:118712. DOI: https://doi.org/10.1016/j.neuroimage.2021.118712, PMID: 34800661

Cohen J. 1988. *Statistical Power Analysis for the Behavioral Sciences*. Routledge.

Colclough GL, Brookes MJ, Smith SM, Woolrich MW. 2015. A symmetric multivariate leakage correction for MEG connectomes. *NeuroImage* **117**:439–448. DOI: https://doi.org/10.1016/j.neuroimage.2015.03.071, PMID: 25862259

Cremers HR, Wager TD, Yarkoni T. 2017. The relation between statistical power and inference in fMRI. *PLOS ONE* **12**:e0184923. DOI: https://doi.org/10.1371/journal.pone.0184923, PMID: 29155843

Cummins TDR, Finnigan S. 2007. Theta power is reduced in healthy cognitive aging. *International Journal of Psychophysiology* **66**:10–17. DOI: https://doi.org/10.1016/j.ijpsycho.2007.05.008, PMID: 17582632

Cusack R, Vicente-Grabovetsky A, Mitchell DJ, Wild CJ, Auer T, Linke AC, Peelle JE. 2014. Automatic analysis (aa): efficient neuroimaging workflows and parallel processing using Matlab and XML. *Frontiers in Neuroinformatics* **8**:90. DOI: https://doi.org/10.3389/fninf.2014.00090, PMID: 25642185

Dafflon J, F Da Costa P, Váša F, Monti RP, Bzdok D, Hellyer PJ, Turkheimer F, Smallwood J, Jones E, Leech R. 2022. A guided multiverse study of neuroimaging analyses. *Nature Communications* **13**:3758. DOI: https://doi.org/10.1038/s41467-022-31347-8, PMID: 35768409

Dammers J, Schiek M, Boers F, Silex C, Zvyagintsev M, Pietrzyk U, Mathiak K. 2008. Integration of amplitude and phase statistics for complete artifact removal in independent components of neuromagnetic recordings. *IEEE Transactions on Bio-Medical Engineering* **55**:2353–2362. DOI: https://doi.org/10.1109/TBME.2008.926677, PMID: 18838360

Dave S, Brothers TA, Swaab TY. 2018. 1/f neural noise and electrophysiological indices of contextual prediction in aging. *Brain Research* **1691**:34–43. DOI: https://doi.org/10.1016/j.brainres.2018.04.007, PMID: 29679544

de Cheveigné A. 2020. ZapLine: A simple and effective method to remove power line artifacts. *NeuroImage* **207**:116356. DOI: https://doi.org/10.1016/j.neuroimage.2019.116356, PMID: 31786167

Donoghue T, Haller M, Peterson EJ, Varma P, Sebastian P, Gao R, Noto T, Lara AH, Wallis JD, Knight RT, Shestyuk A, Voytek B. 2020. Parameterizing neural power spectra into periodic and aperiodic components. *Nature Neuroscience* **23**:1655–1665. DOI: https://doi.org/10.1038/s41593-020-00744-x, PMID: 33230329

Donoghue T, Schaworonkow N, Voytek B. 2021. Methodological considerations for studying neural oscillations. *The European Journal of Neuroscience* **55**:3502–3527. DOI: https://doi.org/10.1111/ejn.15361, PMID: 34268825

Dustman RE, Shearer DE, Emmerson RY. 1993. EEG and event-related potentials in normal aging. *Progress in Neurobiology* **41**:369–401. DOI: https://doi.org/10.1016/0301-0082(93)90005-d, PMID: 8210412

Ellekjær H, Holmen J, Indredavik B, Terent A. 1997. Epidemiology of stroke in innherred, norway, 1994 to 1996. *Stroke* **28**:2180–2184. DOI: https://doi.org/10.1161/01.STR.28.11.2180, PMID: 9368561

Feigin VL, Forouzanfar MH, Krishnamurthi R, Mensah GA, Connor M, Bennett DA, Moran AE, Sacco RL, Anderson L, Truelsen T, O'Donnell M, Venketasubramanian N, Barker-Collo S, Lawes CMM, Wang W,

Shinohara Y, Witt E, Ezzati M, Naghavi M, Murray C. 2014. Global and regional burden of stroke during 1990–2010: findings from the global burden of disease study 2010. *The Lancet* **383**:245–255. DOI: https://doi.org/10.1016/S0140-6736(13)61953-4, PMID: 24449944

Finley AJ, Angus DJ, Knight EL, van Reekum CM, Lachman ME, Davidson RJ, Schaefer SM. 2024. Resting EEG periodic and aperiodic components predict cognitive decline over 10 years. *The Journal of Neuroscience* **44**:e1332232024. DOI: https://doi.org/10.1523/JNEUROSCI.1332-23.2024, PMID: 38373849

Finnigan S, Robertson IH. 2011. Resting EEG theta power correlates with cognitive performance in healthy older adults. *Psychophysiology* **48**:1083–1087. DOI: https://doi.org/10.1111/j.1469-8986.2010.01173.x, PMID: 21729101

Frangou S, Modabbernia A, Williams SCR, Papachristou E, Doucet GE, Agartz I, Aghajani M, Akudjedu TN, Albajes-Eizagirre A, Alnaes D, Alpert KI, Andersson M, Andreasen NC, Andreassen OA, Asherson P, Banaschewski T, Bargallo N, Baumeister S, Baur-Streubel R, Bertolino A, et al. 2022. Cortical thickness across the lifespan: Data from 17,075 healthy individuals aged 3-90 years. *Human Brain Mapping* **43**:431–451. DOI: https://doi.org/10.1002/hbm.25364, PMID: 33595143

Freschl J, Azizi LA, Balboa L, Kaldy Z, Blaser E. 2022. The development of peak alpha frequency from infancy to adolescence and its role in visual temporal processing: A meta-analysis. *Developmental Cognitive Neuroscience* **57**:101146. DOI: https://doi.org/10.1016/j.dcn.2022.101146, PMID: 35973361

Garcés P, Vicente R, Wibral M, Pineda-Pardo JÁ, López ME, Aurtenetxe S, Marcos A, de Andrés ME, Yus M, Sancho M, Maestú F, Fernández A. 2013. Brain-wide slowing of spontaneous alpha rhythms in mild cognitive impairment. *Frontiers in Aging Neuroscience* **5**:100. DOI: https://doi.org/10.3389/fnagi.2013.00100, PMID: 24409145

Gelman A, Loken E. 2013. The Garden of Forking Paths: Why Multiple Comparisons Can Be a Problem, Even When There Is No "Fishing Expedition" or "p-Hacking" and the Research Hypothesis Was Posited Ahead of Time. Columbia Statistics. https://sites.stat.columbia.edu/gelman/research/unpublished/p_hacking.pdf

Gómez C, Pérez-Macías JM, Poza J, Fernández A, Hornero R. 2013. Spectral changes in spontaneous MEG activity across the lifespan. *Journal of Neural Engineering* **10**:066006. DOI: https://doi.org/10.1088/1741-2560/10/6/066006, PMID: 24100075

Gorgolewski KJ, Varoquaux G, Rivera G, Schwarz Y, Ghosh SS, Maumet C, Sochat VV, Nichols TE, Poldrack RA, Poline JB, Yarkoni T, Margulies DS. 2015. NeuroVault.org: a web-based repository for collecting and sharing unthresholded statistical maps of the human brain. *Frontiers in Neuroinformatics* **9**:8. DOI: https://doi.org/10.3389/fninf.2015.00008, PMID: 25914639

Gramfort A, Luessi M, Larson E, Engemann DA, Strohmeier D, Brodbeck C, Goj R, Jas M, Brooks T, Parkkonen L, Hämäläinen M. 2013. MEG and EEG data analysis with MNE-Python. *Frontiers in Neuroscience* **7**:267. DOI: https://doi.org/10.3389/fnins.2013.00267, PMID: 24431986

Gross J, Baillet S, Barnes GR, Henson RN, Hillebrand A, Jensen O, Jerbi K, Litvak V, Maess B, Oostenveld R, Parkkonen L, Taylor JR, van Wassenhove V, Wibral M, Schoffelen JM. 2013. Good practice for conducting and reporting MEG research. *NeuroImage* **65**:349–363. DOI: https://doi.org/10.1016/j.neuroimage.2012.10.001, PMID: 23046981

Harris CR, Millman KJ, van der Walt SJ, Gommers R, Virtanen P, Cournapeau D, Wieser E, Taylor J, Berg S, Smith NJ, Kern R, Picus M, Hoyer S, van Kerkwijk MH, Brett M, Haldane A, Del Río JF, Wiebe M, Peterson P, Gérard-Marchant P, et al. 2020. Array programming with NumPy. *Nature* **585**:357–362. DOI: https://doi.org/10.1038/s41586-020-2649-2, PMID: 32939066

Heinrichs-Graham E, Wilson TW. 2016. Is an absolute level of cortical beta suppression required for proper movement? Magnetoencephalographic evidence from healthy aging. *NeuroImage* **134**:514–521. DOI: https://doi.org/10.1016/j.neuroimage.2016.04.032, PMID: 27090351

Heinrichs-Graham E, McDermott TJ, Mills MS, Wiesman AI, Wang YP, Stephen JM, Calhoun VD, Wilson TW. 2018. The lifespan trajectory of neural oscillatory activity in the motor system. *Developmental Cognitive Neuroscience* **30**:159–168. DOI: https://doi.org/10.1016/j.dcn.2018.02.013, PMID: 29525417

Hillebrand A, Singh KD, Holliday IE, Furlong PL, Barnes GR. 2005. A new approach to neuroimaging with magnetoencephalography. *Human Brain Mapping* **25**:199–211. DOI: https://doi.org/10.1002/hbm.20102, PMID: 15846771

Hillebrand A, Gaetz W, Furlong PL, Gouw AA, Stam CJ. 2018. Practical guidelines for clinical magnetoencephalography - Another step towards best practice. *Clinical Neurophysiology* **129**:1709–1711. DOI: https://doi.org/10.1016/j.clinph.2018.05.007, PMID: 29903504

Hoenig JM, Heisey DM. 2001. The abuse of power: the pervasive fallacy of power calculations for data analysis. *The American Statistician* **55**:19–24. DOI: https://doi.org/10.1198/000313001300339897

Hoshi H, Shigihara Y. 2020. Age- and gender-specific characteristics of the resting-state brain activity: a magnetoencephalography study. *Aging* **12**:21613–21637. DOI: https://doi.org/10.18632/aging.103956, PMID: 33147568

Hübner L, Godde B, Voelcker-Rehage C. 2018. Older adults reveal enhanced task-related beta power decreases during a force modulation task. *Behavioural Brain Research* **345**:104–113. DOI: https://doi.org/10.1016/j.bbr.2018.02.028, PMID: 29486269

Hughes LE, Henson RN, Pereda E, Bruña R, López-Sanz D, Quinn AJ, Woolrich MW, Nobre AC, Rowe JB, Maestú F, the BioFIND Working Group. 2019. Biomagnetic biomarkers for dementia: A pilot multicentre study with a recommended methodological framework for magnetoencephalography. *Alzheimer's & Dementia* **11**:450–462. DOI: https://doi.org/10.1016/j.dadm.2019.04.009, PMID: 31431918

Hunter JD. 2007. Matplotlib: a 2D graphics environment. *Computing in Science & Engineering* **9**:90–95. DOI: https://doi.org/10.1109/MCSE.2007.55
Hyvärinen A. 1999. Fast and robust fixed-point algorithms for independent component analysis. *IEEE Transactions on Neural Networks* **10**:626–634. DOI: https://doi.org/10.1109/72.761722, PMID: 18252563
Jabès A, Klencklen G, Ruggeri P, Antonietti JP, Banta Lavenex P, Lavenex P. 2021. Age-related differences in resting-state EEG and allocentric spatial working memory performance. *Frontiers in Aging Neuroscience* **13**:704362. DOI: https://doi.org/10.3389/fnagi.2021.704362, PMID: 34803651
Jenkinson M, Smith S. 2001. A global optimisation method for robust affine registration of brain images. *Medical Image Analysis* **5**:143–156. DOI: https://doi.org/10.1016/s1361-8415(01)00036-6, PMID: 11516708
Jenkinson M, Bannister P, Brady M, Smith S. 2002. Improved optimization for the robust and accurate linear registration and motion correction of brain images. *NeuroImage* **17**:825–841. DOI: https://doi.org/10.1006/nimg.2002.1132, PMID: 12377157
Johnson WE, Li C, Rabinovic A. 2007. Adjusting batch effects in microarray expression data using empirical Bayes methods. *Biostatistics* **8**:118–127. DOI: https://doi.org/10.1093/biostatistics/kxj037, PMID: 16632515
Klimesch W. 1999. EEG alpha and theta oscillations reflect cognitive and memory performance: a review and analysis. *Brain Research. Brain Research Reviews* **29**:169–195. DOI: https://doi.org/10.1016/s0165-0173(98)00056-3
Kohl O, Woolrich M, Nobre AC, Quinn A. 2023. Glasser52: a parcellation for MEG-analysis. Zenodo. https://doi.org/10.5281/zenodo.10401792
Koyama K, Hirasawa H, Okubo Y, Karasawa A. 1997. Quantitative EEG correlates of normal aging in the elderly. *Clinical EEG* **28**:160–165. DOI: https://doi.org/10.1177/155005949702800308, PMID: 9241470
Kumar WS, Ray S. 2023. Healthy ageing and cognitive impairment alter EEG functional connectivity in distinct frequency bands. *The European Journal of Neuroscience* **58**:3432–3449. DOI: https://doi.org/10.1111/ejn.16114, PMID: 37559505
Lakens D. 2022. Sample size justification. *Collabra* **8**:33267. DOI: https://doi.org/10.1525/collabra.33267
Lakens D. 2024. When and how to deviate from a preregistration. *Collabra* **10**:2024. DOI: https://doi.org/10.1525/collabra.117094
Lejko N, Larabi DI, Herrmann CS, Aleman A, Ćurčić-Blake B. 2020. Alpha power and functional connectivity in cognitive decline: a systematic review and meta-analysis. *Journal of Alzheimer's Disease* **78**:1047–1088. DOI: https://doi.org/10.3233/JAD-200962, PMID: 33185607
Lenth RV. 2001. Some practical guidelines for effective sample size determination. *The American Statistician* **55**:187–193. DOI: https://doi.org/10.1198/000313001317098149
Litvak V, Mattout J, Kiebel S, Phillips C, Henson R, Kilner J, Barnes G, Oostenveld R, Daunizeau J, Flandin G, Penny W, Friston K. 2011. EEG and MEG data analysis in SPM8. *Computational Intelligence and Neuroscience* **2011**:852961. DOI: https://doi.org/10.1155/2011/852961, PMID: 21437221
Lodder SS, van Putten M. 2011. Automated EEG analysis: characterizing the posterior dominant rhythm. *Journal of Neuroscience Methods* **200**:86–93. DOI: https://doi.org/10.1016/j.jneumeth.2011.06.008, PMID: 21722667
López-Otín C, Blasco MA, Partridge L, Serrano M, Kroemer G. 2013. The Hallmarks of Aging. *Cell* **153**:1194–1217. DOI: https://doi.org/10.1016/j.cell.2013.05.039
López-Sanz D, Bruña R, Garcés P, Camara C, Serrano N, Rodríguez-Rojo IC, Delgado ML, Montenegro M, López-Higes R, Yus M, Maestú F. 2016. Alpha band disruption in the AD-continuum starts in the Subjective Cognitive Decline stage: a MEG study. *Scientific Reports* **6**:37685. DOI: https://doi.org/10.1038/srep37685
Maestú F, Fernández A. 2020. Role of magnetoencephalography in the early stages of alzheimer disease. *Neuroimaging Clinics of North America* **30**:217–227. DOI: https://doi.org/10.1016/j.nic.2020.01.003, PMID: 32336408
Mahjoory K, Schoffelen JM, Keitel A, Gross J. 2020. The frequency gradient of human resting-state brain oscillations follows cortical hierarchies. *eLife* **9**:e53715. DOI: https://doi.org/10.7554/eLife.53715, PMID: 32820722
Medrano J, Alexander NA, Seymour RA, Zeidman P. 2025. BSD: a bayesian framework for parametric models of neural spectra. *The European Journal of Neuroscience* **61**:e70149. DOI: https://doi.org/10.1111/ejn.70149, PMID: 40415547
Merkin A, Sghirripa S, Graetz L, Smith AE, Hordacre B, Harris R, Pitcher J, Semmler J, Rogasch NC, Goldsworthy M. 2023. Do age-related differences in aperiodic neural activity explain differences in resting EEG alpha? *Neurobiology of Aging* **121**:78–87. DOI: https://doi.org/10.1016/j.neurobiolaging.2022.09.003, PMID: 36379095
Meteyard L, Davies RAI. 2020. Best practice guidance for linear mixed-effects models in psychological science. *Journal of Memory and Language* **112**:104092. DOI: https://doi.org/10.1016/j.jml.2020.104092
Mumford JA. 2012. A power calculation guide for fMRI studies. *Social Cognitive and Affective Neuroscience* **7**:738–742. DOI: https://doi.org/10.1093/scan/nss059, PMID: 22641837
Murty D, Manikandan K, Kumar WS, Ramesh RG, Purokayastha S, Javali M, Rao NP, Ray S. 2020. Gamma oscillations weaken with age in healthy elderly in human EEG. *NeuroImage* **215**:116826. DOI: https://doi.org/10.1016/j.neuroimage.2020.116826, PMID: 32276055
Nosek BA, Errington TM. 2020. What is replication? *PLOS Biology* **18**:e3000691. DOI: https://doi.org/10.1371/journal.pbio.3000691, PMID: 32218571
Nosek BA, Hardwicke TE, Moshontz H, Allard A, Corker KS, Dreber A, Fidler F, Hilgard J, Kline Struhl M, Nuijten MB, Rohrer JM, Romero F, Scheel AM, Scherer LD, Schönbrodt FD, Vazire S. 2022. replicability,

robustness, and reproducibility in psychological science. *Annual Review of Psychology* **73**:719–748. DOI: https://doi.org/10.1146/annurev-psych-020821-114157, PMID: 34665669

Osipova D, Ahveninen J, Jensen O, Ylikoski A, Pekkonen E. 2005. Altered generation of spontaneous oscillations in Alzheimer's disease. *NeuroImage* **27**:835–841. DOI: https://doi.org/10.1016/j.neuroimage.2005.05.011, PMID: 15961323

Park J, Ho RLM, Wang W-E, Nguyen VQ, Coombes SA. 2024. The effect of age on alpha rhythms in the human brain derived from source localized resting-state electroencephalography. *NeuroImage* **292**:120614. DOI: https://doi.org/10.1016/j.neuroimage.2024.120614, PMID: 38631618

Patenaude B, Smith SM, Kennedy DN, Jenkinson M. 2011. A Bayesian model of shape and appearance for subcortical brain segmentation. *NeuroImage* **56**:907–922. DOI: https://doi.org/10.1016/j.neuroimage.2011.02.046, PMID: 21352927

Pathak A, Sharma V, Roy D, Banerjee A. 2022. Biophysical mechanism underlying compensatory preservation of neural synchrony over the adult lifespan. *Communications Biology* **5**:567. DOI: https://doi.org/10.1038/s42003-022-03489-4, PMID: 35681107

Penrose R. 1956. On best approximate solutions of linear matrix equations. *Mathematical Proceedings of the Cambridge Philosophical Society* **52**:17–19. DOI: https://doi.org/10.1017/S0305004100030929

Pernet CR, Garrido M, Gramfort A, Maurits N, Michel C, Pang E, Salmelin R, Schoffelen JM, Valdes-Sosa PA, Puce A. 2018. Best practices in data analysis and sharing in neuroimaging using MEEG. Open Science Framework. https://osf.io/a8dhx_v1

Perrin F, Pernier J, Bertrand O, Echallier JF. 1989. Spherical splines for scalp potential and current density mapping. *Electroencephalography and Clinical Neurophysiology* **72**:184–187. DOI: https://doi.org/10.1016/0013-4694(89)90180-6, PMID: 2464490

Planche V, Manjon JV, Mansencal B, Lanuza E. 2022. Structural progression of Alzheimer's disease over decades: the MRI staging scheme. *Brain Communications* **4**:fcac109. DOI: https://doi.org/10.1093/braincomms/fcac109, PMID: 35592489

Power L, Allain C, Moreau T, Gramfort A, Bardouille T. 2023. Using convolutional dictionary learning to detect task-related neuromagnetic transients and ageing trends in a large open-access dataset. *NeuroImage* **267**:119809. DOI: https://doi.org/10.1016/j.neuroimage.2022.119809, PMID: 36584759

Puttaert D, Wens V, Fery P, Rovai A, Trotta N, Coquelet N, De Breucker S, Sadeghi N, Coolen T, Goldman S, Peigneux P, Bier JC, De Tiège X. 2021. Decreased alpha peak frequency is linked to episodic memory impairment in pathological aging. *Frontiers in Aging Neuroscience* **13**:711375. DOI: https://doi.org/10.3389/fnagi.2021.711375, PMID: 34475819

Quinn A, Hymers M. 2020. SAILS: spectral analysis in linear systems. *Journal of Open Source Software* **5**:1982. DOI: https://doi.org/10.21105/joss.01982

Quinn AJ, Green GGR, Hymers M. 2021. Delineating between-subject heterogeneity in alpha networks with Spatio-Spectral Eigenmodes. *NeuroImage* **240**:118330. DOI: https://doi.org/10.1016/j.neuroimage.2021.118330, PMID: 34237443

Quinn AJ, Gohil C, Woolrich MW. 2022. OHBA software library in python. Zenodo. https://doi.org/10.5281/zenodo.6875059

Quinn AJ, Atkinson LZ, Gohil C, Kohl O, Pitt J, Zich C, Nobre AC, Woolrich MW. 2024. The GLM-spectrum: A multilevel framework for spectrum analysis with covariate and confound modelling. *Imaging Neuroscience* **2**:1–26. DOI: https://doi.org/10.1162/imag_a_00082, PMID: 40800496

Quinn AJ. 2025. Quinn2025-robustreplicableage. swh:1:rev:8508158bafebe6de19266c184d2d30bbb64202f6. Software Heritage. https://archive.softwareheritage.org/swh:1:dir:a9c001a1f4e5e7331c164f8fd3fbc6d84c009420;origin=https://github.com/OHBA-analysis/Quinn2025-RobustReplicableAge;visit=swh:1:snp:c3ae2e5e2f6cd970f2760b826f824d817888082a;anchor=swh:1:rev:8508158bafebe6de19266c184d2d30bbb64202f6

Reddan MC, Lindquist MA, Wager TD. 2017. Effect size estimation in neuroimaging. *JAMA Psychiatry* **74**:207–208. DOI: https://doi.org/10.1001/jamapsychiatry.2016.3356, PMID: 28099973

Rempe MP, Ott LR, Picci G, Penhale SH, Christopher-Hayes NJ, Lew BJ, Petro NM, Embury CM, Schantell M, Johnson HJ, Okelberry HJ, Losh KL, Willett MP, Losh RA, Wang YP, Calhoun VD, Stephen JM, Heinrichs-Graham E, Kurz MJ, Wilson TW. 2023. Spontaneous cortical dynamics from the first years to the golden years. *PNAS* **120**:e2212776120. DOI: https://doi.org/10.1073/pnas.2212776120, PMID: 36652485

Rosner B. 1983. Percentage points for a generalized ESD many-outlier procedure. *Technometrics* **25**:165–172. DOI: https://doi.org/10.1080/00401706.1983.10487848

Rossiter HE, Davis EM, Clark EV, Boudrias MH, Ward NS. 2014. Beta oscillations reflect changes in motor cortex inhibition in healthy ageing. *NeuroImage* **91**:360–365. DOI: https://doi.org/10.1016/j.neuroimage.2014.01.012, PMID: 24440529

Sahoo B, Pathak A, Deco G, Banerjee A, Roy D. 2020. Lifespan associated global patterns of coherent neural communication. *NeuroImage* **216**:116824. DOI: https://doi.org/10.1016/j.neuroimage.2020.116824, PMID: 32289459

Sandre A, Troller-Renfree SV. 2026. Power struggles: Absolute vs. relative EEG power in developmental neuroscience. *Developmental Cognitive Neuroscience* **79**:101698. DOI: https://doi.org/10.1016/j.dcn.2026.101698, PMID: 41795501

Scally B, Burke MR, Bunce D, Delvenne JF. 2018. Resting-state EEG power and connectivity are associated with alpha peak frequency slowing in healthy aging. *Neurobiology of Aging* **71**:149–155. DOI: https://doi.org/10.1016/j.neurobiolaging.2018.07.004, PMID: 30144647

Selya AS, Rose JS, Dierker LC, Hedeker D, Mermelstein RJ. 2012. A practical guide to calculating cohen's f(2), a measure of local effect size, from PROC MIXED. *Frontiers in Psychology* **3**:111. DOI: https://doi.org/10.3389/fpsyg.2012.00111, PMID: 22529829

Shafto MA, Tyler LK, Dixon M, Taylor JR, Rowe JB, Cusack R, Calder AJ, Marslen-Wilson WD, Duncan J, Dalgleish T, Henson RN, Brayne C, Matthews FE, Cam-CAN. 2014. The cambridge centre for ageing and neuroscience (Cam-CAN) study protocol: a cross-sectional, lifespan, multidisciplinary examination of healthy cognitive ageing. *BMC Neurology* **14**:204. DOI: https://doi.org/10.1186/s12883-014-0204-1, PMID: 25412575

Shafto MA, Henson RN, Matthews FE, Taylor JR, Emery T, Erzinclioglu S, Hanley C, Rowe JB, Cusack R, Calder AJ, Marslen-Wilson WD, Duncan J, Dalgleish T, Brayne C, Tyler LK. 2020. Cognitive diversity in a healthy aging cohort: cross-domain cognition in the cam-CAN project. *Journal of Aging and Health* **32**:1029–1041. DOI: https://doi.org/10.1177/0898264319878095, PMID: 31592706

Smith SM. 2002. Fast robust automated brain extraction. *Human Brain Mapping* **17**:143–155. DOI: https://doi.org/10.1002/hbm.10062, PMID: 12391568

Smith SM, Nichols TE. 2018. Statistical challenges in "big data" human neuroimaging. *Neuron* **97**:263–268. DOI: https://doi.org/10.1016/j.neuron.2017.12.018, PMID: 29346749

Sokoliuk R, Mayhew SD, Aquino KM, Wilson R, Brookes MJ, Francis ST, Hanslmayr S, Mullinger KJ. 2019. Two spatially distinct posterior alpha sources fulfill different functional roles in attention. *The Journal of Neuroscience* **39**:7183–7194. DOI: https://doi.org/10.1523/JNEUROSCI.1993-18.2019, PMID: 31341028

Stier C, Braun C, Focke NK. 2023. Adult lifespan trajectories of neuromagnetic signals and interrelations with cortical thickness. *NeuroImage* **278**:120275. DOI: https://doi.org/10.1016/j.neuroimage.2023.120275, PMID: 37451375

Stier C, Balestrieri E, Fehring J, Focke NK, Wollbrink A, Dannlowski U, Gross J. 2024. Extensive MEG time-series phenotyping unveils neural markers predictive of age. *bioRxiv*. DOI: https://doi.org/10.1101/2024.05.09.593348

Taulu S, Kajola M. 2005. Presentation of electromagnetic multichannel data: The signal space separation method. *Journal of Applied Physics* **97**:124905. DOI: https://doi.org/10.1063/1.1935742

Taulu S, Simola J. 2006. Spatiotemporal signal space separation method for rejecting nearby interference in MEG measurements. *Physics in Medicine and Biology* **51**:1759–1768. DOI: https://doi.org/10.1088/0031-9155/51/7/008, PMID: 16552102

Taylor JR, Williams N, Cusack R, Auer T, Shafto MA, Dixon M, Tyler LK, Henson RN. 2017. The cambridge centre for ageing and neuroscience (Cam-CAN) data repository: Structural and functional MRI, MEG, and cognitive data from a cross-sectional adult lifespan sample. *NeuroImage* **144**:262–269. DOI: https://doi.org/10.1016/j.neuroimage.2015.09.018, PMID: 26375206

Thuwal K, Banerjee A, Roy D. 2021. Aperiodic and periodic components of ongoing oscillatory brain dynamics link distinct functional aspects of cognition across adult lifespan. *eNeuro* **8**:ENEURO.0224-21.2021. DOI: https://doi.org/10.1523/ENEURO.0224-21.2021, PMID: 34544762

Tröndle M, Popov T, Pedroni A, Pfeiffer C, Barańczuk-Turska Z, Langer N. 2023. Decomposing age effects in EEG alpha power. *Cortex* **161**:116–144. DOI: https://doi.org/10.1016/j.cortex.2023.02.002, PMID: 36933455

Turner C, Baylan S, Bracco M, Cruz G, Hanzal S, Keime M, Kuye I, McNeill D, Ng Z, van der Plas M, Ruzzoli M, Thut G, Trajkovic J, Veniero D, Wale SP, Whear S, Learmonth G. 2023. Developmental changes in individual alpha frequency: Recording EEG data during public engagement events. *Imaging Neuroscience* **1**:1–14. DOI: https://doi.org/10.1162/imag_a_00001, PMID: 37719836

Ustinin M, Boyko A, Rykunov S. 2025. Healthy aging changes in conventional frequency bands of neuroelectric brain activity reconstructed from resting-state MEG. *GeroScience* **47**:4093–4108. DOI: https://doi.org/10.1007/s11357-025-01522-y, PMID: 39821802

van Es MWJ, Gohil C, Quinn AJ, Woolrich MW. 2025. osl-ephys: a Python toolbox for the analysis of electrophysiology data. *Frontiers in Neuroscience* **19**:1522675. DOI: https://doi.org/10.3389/fnins.2025.1522675, PMID: 40061258

Van Veen BD, Buckley KM. 1988. Beamforming: a versatile approach to spatial filtering. *IEEE ASSP Magazine* **5**:4–24. DOI: https://doi.org/10.1109/53.665

Veldhuizen RJ, Jonkman EJ, Poortvliet DCJ. 1993. Sex differences in age regression parameters of healthy adults--normative data and practical implications. *Electroencephalography and Clinical Neurophysiology* **86**:377–384. DOI: https://doi.org/10.1016/0013-4694(93)90133-g, PMID: 7686472

Virtanen P, Gommers R, Oliphant TE, Haberland M, Reddy T, Cournapeau D, Burovski E, Peterson P, Weckesser W, Bright J, van der Walt SJ, Brett M, Wilson J, Millman KJ, Mayorov N, Nelson ARJ, Jones E, Kern R, Larson E, Carey CJ, et al. 2020. Author Correction: SciPy 1.0: fundamental algorithms for scientific computing in Python. *Nature Methods* **17**:352. DOI: https://doi.org/10.1038/s41592-020-0772-5, PMID: 32094914

Vlahou EL, Thurm F, Kolassa IT, Schlee W. 2014. Resting-state slow wave power, healthy aging and cognitive performance. *Scientific Reports* **4**:5101. DOI: https://doi.org/10.1038/srep05101, PMID: 24869503

Voytek B, Kramer MA, Case J, Lepage KQ, Tempesta ZR, Knight RT, Gazzaley A. 2015. Age-related changes in 1/f neural electrophysiological noise. *The Journal of Neuroscience* **35**:13257–13265. DOI: https://doi.org/10.1523/JNEUROSCI.2332-14.2015, PMID: 26400953

Vysata O, Kukal J, Prochazka A, Pazdera L, Valis M. 2012. Age-related changes in the energy and spectral composition of EEG. *Neurophysiology* **44**:63–67. DOI: https://doi.org/10.1007/s11062-012-9268-y

Woolrich MW, Jbabdi S, Patenaude B, Chappell M, Makni S, TimothyBehrens CB, Jenkinson M, Smith SM. 2009. Bayesian analysis ofneuroimaging data in FSL. *NeuroImage* **45**:S173–S186. DOI: https://doi.org/10.1016/j.neuroimage.2008.10.055

World Health Organization. 2015. World report on ageing and health. https://iris.who.int/handle/10665/186463 [Accessed October 13, 2024].

Xifra-Porxas A, Niso G, Larivière S, Kassinopoulos M, Baillet S, Mitsis GD, Boudrias MH. 2019. Older adults exhibit a more pronounced modulation of beta oscillations when performing sustained and dynamic handgrips. *NeuroImage* **201**:116037. DOI: https://doi.org/10.1016/j.neuroimage.2019.116037, PMID: 31330245

Zhang Y, Brady M, Smith S. 2001. Segmentation of brain MR images through a hidden Markovrandom field model and the expectation-maximization algorithm. *IEEE Transactions on MedicalImaging* **20**:45–57. DOI: https://doi.org/10.1109/42.906424, PMID: 11293691

Zibrandtsen IC, Kjaer TW. 2021. Fully automatic peak frequency estimation of the posterior dominant rhythm in a large retrospective hospital EEG cohort. *Clinical Neurophysiology Practice* **6**:1–9. DOI: https://doi.org/10.1016/j.cnp.2020.11.001, PMID: 33385100

Appendix 1

Literature review of alpha effects

Part of our motivation for this method is that variability in the methodological choices made in different publications makes it difficult to aggregate varying results across the literature. For example, though decrease in alpha peak frequency with increasing age is reported highly consistently, the effect of age on alpha power is much more variable. ***Appendix 1—table 1*** shows a sample of publications over the last 20 years that report a change in alpha power with age (note that this is intended to be a representative rather than an exhaustive list). Over half of publications (9/15) report a decrease in alpha power whilst the remaining publications report an increase (2/15), both increases and decreases (1/15), a decrease but only without correcting for aperiodic slope (1/15), a quadratic effect (1/15), and no-effect (1/15). ***Stier et al., 2023***, suggest that the choice of analysis space (sensor space or source reconstruction) might drive these differences.

Critically, it is difficult to reconcile these findings with the information reported in the publications. For example, even within the nine publications that report a decrease, there is little correspondence in the spatial location of the effect. We argue that focused approaches cannot resolve this issue alone as targeted analyses are more specific to each dataset and less generalisable.

In the specific case of the mixed literature on change in alpha power with age, our results show that both effects are present and separated in frequency. It is feasible that the different methodological choices and datasets used by each study in our survey means that one or other of these two effects were emphasised. As a result, the literature may not be mixed in scientific terms, but that a rich pattern of results is obscured by methodological variability.

Appendix 1—table 1. A selection of publications from the last 20 years reporting age-dependent differences in alpha power.

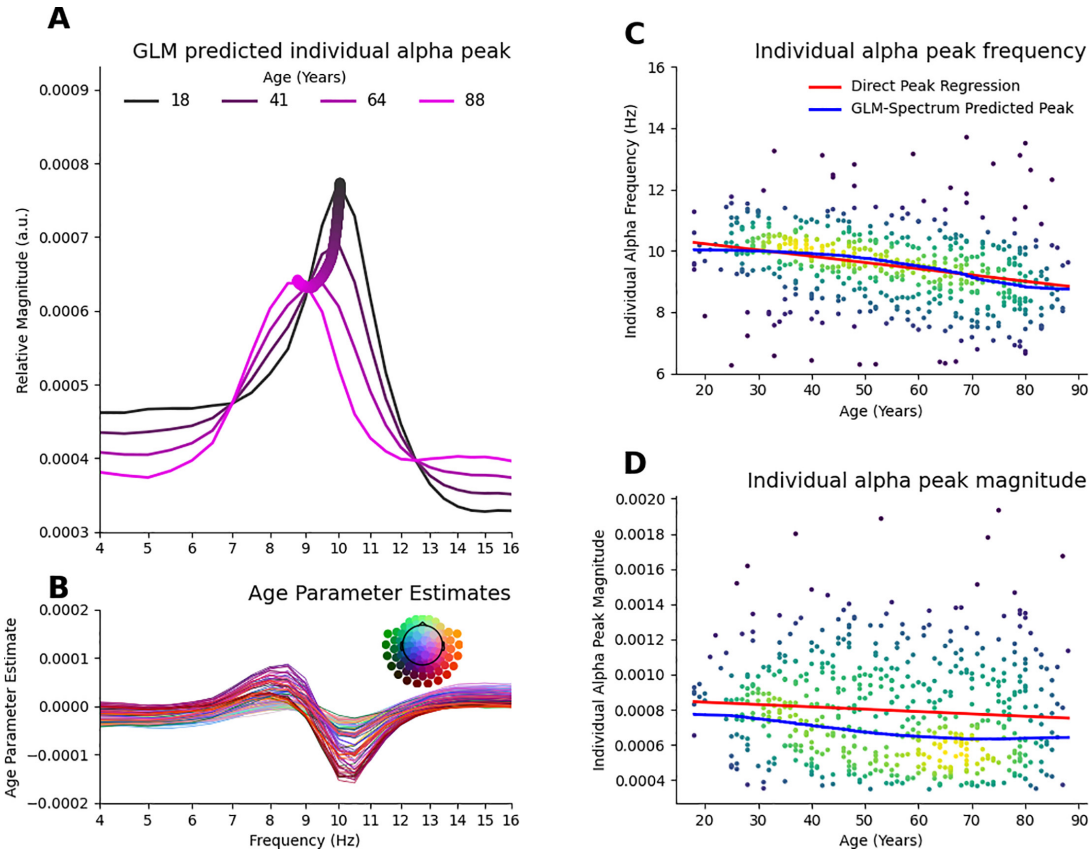
A variety of methodological approaches are used by the papers. Note that this is not intended to be a comprehensive list of all publications in this time, but is a representative sample of the variability in methods and results found in the literature.

Publication	Method/alpha frequency/location	Change with age	Figure in source publication
Babiloni et al., 2006	Method: MEG source space Alpha: 8–10.5 Hz; 10.5–13 Hz Peak: parietal, occipital, temporal, limbic areas	Decrease	Figures 1, 2 & 3
Lodder and van Putten, 2011	Method: EEG sensor space Alpha: individual peak (3–18 Hz) Peak: individual peak	Decrease	Table 2
Vysata et al., 2012	Method: EEG sensor space Alpha: 7–13 Hz Peak: whole head	Decrease	Figure 2
Gómez et al., 2013	Method: MEG sensor space Alpha: 8–13 Hz Peak: parieto-temporal areas	Quadratic	Figure 3
Scally et al., 2018	Method: EEG sensor space Alpha: individual peak (6–14 Hz) and upper alpha (10–12 Hz) Peak: all channels averaged	No change (individual) Decrease (upper alpha)	Figure 5
Hoshi and Shigihara, 2020	Method: MEG source space Alpha: 8–12 Hz Peak: temporal pole; visual cortex V1–V4	Increase (TP) Decrease (visual)	Table 3
Donoghue et al., 2020	Method: EEG sensor space Alpha: individual peak (7–14 Hz) Peak: sensor Oz	Decrease	Figure 5

Appendix 1—table 1 Continued on next page

Appendix 1—table 1 Continued

Publication	Method/alpha frequency/location	Change with age	Figure in source publication
Thuwal et al., 2021	Method: MEG sensor space Alpha: individual peak (8–12 Hz) Peak: occipito-parietal sensors	Decrease	Figure 6
Rempe et al., 2023	Method: MEG source space Alpha: 8–12 Hz Peak: bilateral inferior temporal gyrus	Increase	Figures 2 & 3
Stier et al., 2023	Method: MEG source space Alpha: 8–12 Hz Peak: temporal regions	Increase	Figure 2
Merkin et al., 2023	Method: EEG sensor space Alpha: individual peak (after 1/*f* correction) Peak: all channels	No change	Figure 3
Tröndle et al., 2023	Method: EEG sensor space Alpha:individual peak ± 2 Hz (8–13 Hz) Peak: parietal and occipital	Decrease	Figures 5 & 7
Park et al., 2024	Method: EEG source space Alpha: individual peak (6–14 Hz; after 1/*f* correction) Peak: sensorimotor and parietal regions	Decrease	Figures 2 & 3
Ustinin et al., 2025	Method: MEG sensor space Alpha: 8–13 Hz Peak: whole head	Decrease	Figures 5 & 6
Medrano et al., 2025	Method: EEG sensor space Alpha: individual peak (8–12 Hz; after 1/*f* correction) Peak: channel Oz	Decrease	Figure 8



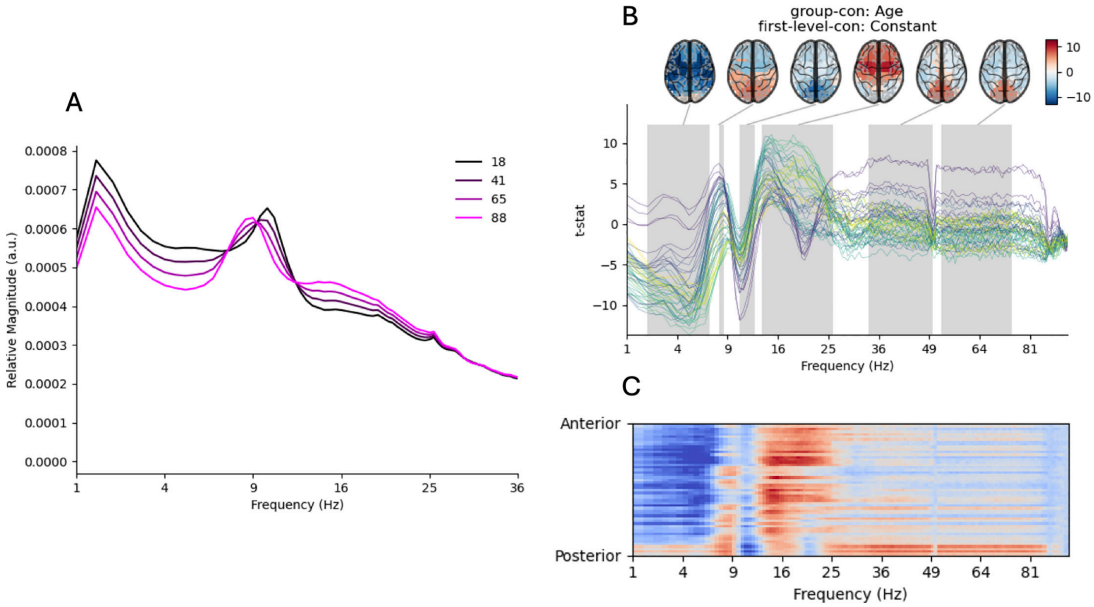
Appendix 1—figure 1. Model projected age effect retains non-linear properties of decrease in alpha peak frequency and magnitude. (**A**) Model-predicted spectra (averaged across all sensors) for the oldest and youngest participants in Cam-CAN with the alpha peak for intermediate ages overlaid in the thick line. (**B**) The parameter estimates of age that combine to describe the peak frequency shift seen in (A). (**C**) Scatter plot of individual alpha peak frequencies against age. A linear regression line fitted directly to the individual alpha peaks is shown in red, and the GLM-Spectrum-derived alpha peaks from the model projected spectra is shown in blue. (**D**) As (C) for individual alpha peak magnitude.

Importantly, the differences in alpha power may be explainable with the change in alpha frequency. Though this was not explicitly modelled by our analysis, it can be visualised by quantifying the alpha peak in the model fitted spectra. A strong reduction in alpha peak frequency is qualitatively visible in the model projected power spectrum (***Appendix 1—figure 1A***). Whilst no single parameter directly fits this feature in the GLM-Spectrum, this pattern is captured by the profile of linear parameters across channels and frequencies. This pattern contains both an increase and a decrease in magnitude with age, separated by frequency (***Appendix 1—figure 1B***). The decrease in alpha peak frequency can be recovered by extrema detection carried out on the model-projected spectra (***Appendix 1—figure 1A***) and shows a prominent decrease in alpha power and alpha frequency across the course of ageing. Critically, by the full profile of parameter estimates, the shape of overall spectrum can represent non-linear changes features that are derived from the full spectrum (***Appendix 1—figure 1C and D***).

Appendix 2

Source space age effect

The sensor space effect shown in ***Appendix 2—figure 1*** is replicated in a source projected analysis using an LCMV beamformer with voxel data organised into parcels that are orthogonalised. The average profile of the age effect in source space is highly consistent with the sensor space result.



Appendix 2—figure 1. Effect of age on the relative magnitude spectrum across space and frequency in linearly constrained minimum variance (LCMV) source reconstructed and parcellated data. (**A**) Model-predicted spectra (averaged across all sensors) for four equally spaced ages across the participant age range. (**B**) Spectrum of t-values quantifying the age effect across space and frequency. Source topographies are shown in the frequency bands with significant effects at sensor space. The permutation statistics are not repeated at source space. (**C**) A 2D frequency-by-space map of all statistically significant effects. Sensor-frequency combinations that do not reach statistical significance have a faded colour scale. Blue regions indicate decreasing spectral power with age, and red regions indicate increases.

Appendix 3

Effect of ICA denoising on the age effect

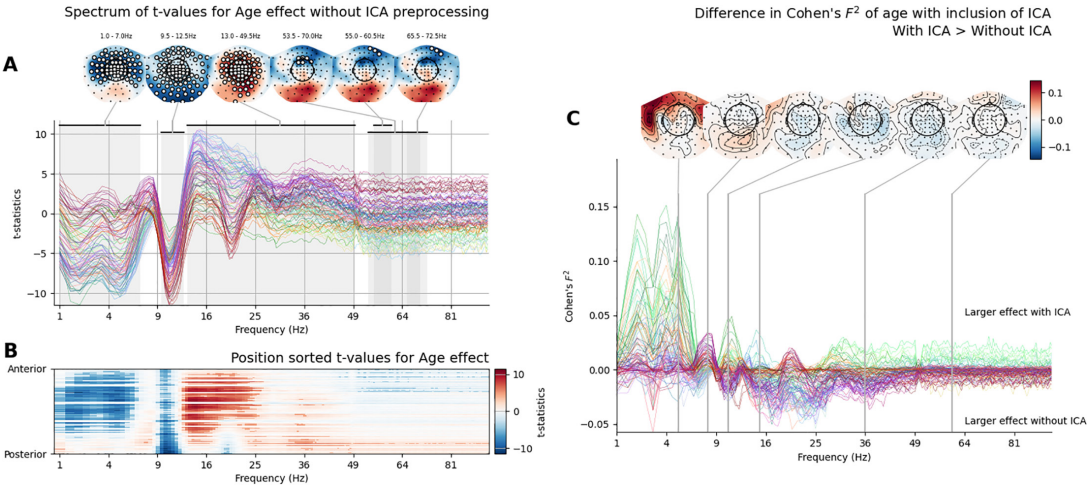
The age results may be contaminated in some way by residual cardiac or ocular artefacts that are not removed during pre-processing. Though ICA denoising was applied, it is possible that some artefactual components were not identified and removed from the dataset. The results at low frequencies and in the gamma range are most likely to be directly impacted by this contamination.

To explore the impact this has on our analysis, we reran the core GLM effect of age on the data with no ICA artefact rejection at all, allowing all eye movements and heart rate components to remain in the data (***Appendix 3—figure 1***).

This no-ICA has three differences to the original in the publication: the low-frequency decrease with age is stronger and more widespread in the analysis that removes ocular artefacts with ICA. A large negative effect is visible in both analyses, though without ICA several frontal and temporal sensors no longer show significant effects. Similarly, the effect size of the low-frequency effect of age is substantially larger when ICA denoising is applied.

The low alpha effect was strongly reduced in the analyses that do not remove artefacts with ICA. A large central-occipital group of sensors show an effect between 7 and 8.5 Hz in the ICA, but this is reduced to a single sensor at 8 Hz when ICA is not computed. At high frequencies, the age effect in frontal sensors is larger with ICA and the age effect in posterior sensors is larger without ICA, though the position and frequencies of significant effects are largely unchanged. The remaining effects in the high alpha and beta ranges are unchanged by the application of ICA.

Overall, ICA either improves the estimation of age effects (low-frequency, low-alpha, high-gamma) or has negligible effect (high-alpha, beta). Only the posterior low-gamma effect is reduced by ICA. Together, we take this as evidence that our core results are robust to interference by eye movements and that the ICA denoising is working effectively to reduce noise in the analysis.



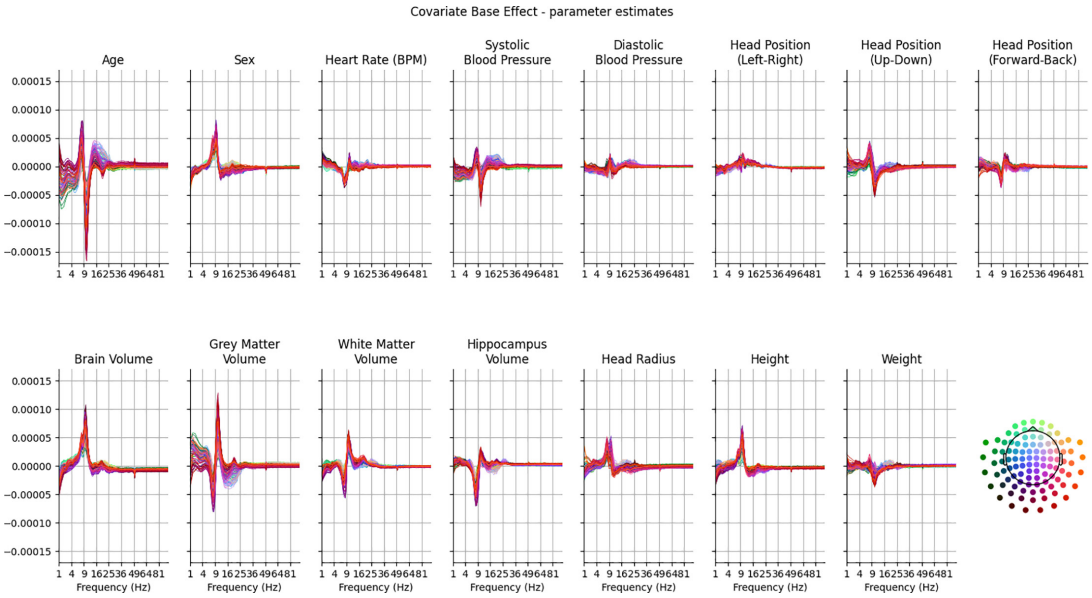
Appendix 3—figure 1. Effect of age with and without independent component analysis (ICA) denoising is largely consistent. (**A**) Spectrum of t-values quantifying the age effect across space and frequency. Non-parametric permutations with maximum statistics to control for multiple comparisons across sensors and frequency bins. While this permutation testing was not cluster-based, contiguous clusters of significant sensors were computed post hoc for visualisation. The largest six spatially and spectrally contiguous areas of statistically significant effects are highlighted in frequency by black bands at the top of the spectrum and highlighted in space by sensors marked with a white circle in the adjoining topography. (**B**) A 2D frequency-by-space map of all statistically significant effects. Sensor-frequency combinations that do not reach statistical significance have a faded colour scale. Blue regions indicate decreasing spectral power with age and red regions indicate increases. (**C**) Spectrum of the difference in estimated effect size of age in data that has been cleaned with ICA and data that has not been cleaned with ICA. Positive values indicate that the effect was larger with ICA denoising and negative values indicate that the effect was smaller with ICA.

Appendix 4

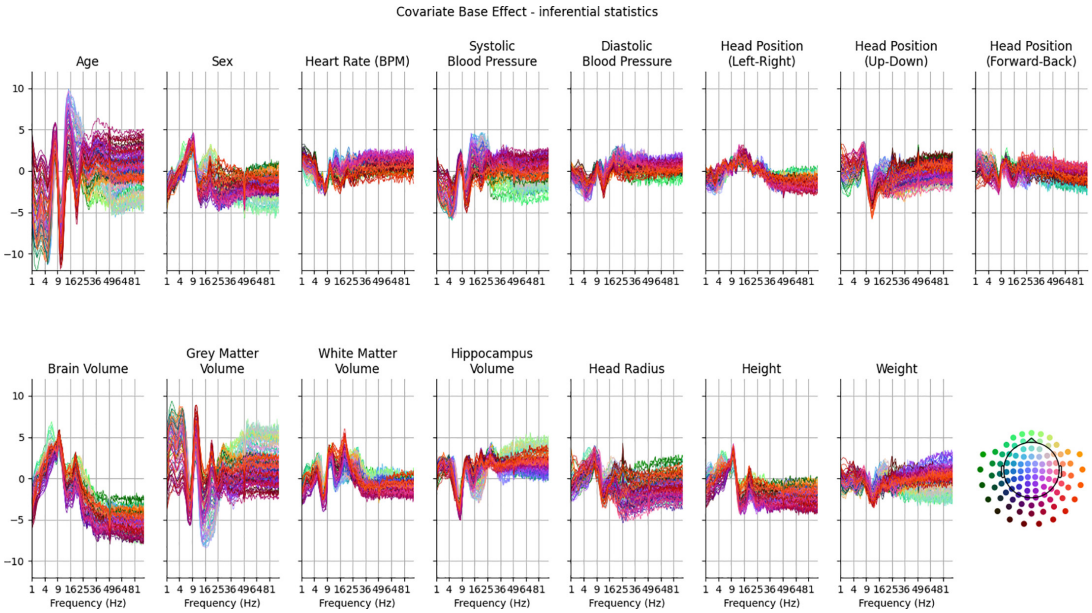
Details of covariate analyses

The GLM-Spectrum effects of the investigated covariate effects are summarised in ***Figure 7*** and shown here in full detail. ***Appendix 4—figures 1–3*** show the results for models fitted with an intercept term and the z-transformed covariate. The full GLM-Spectrum is shown for the parameter estimates (***Appendix 4—figure 1***), t-statistics (***Appendix 4—figure 2***), and Cohen's F^2 effect sizes (***Appendix 4—figure 3***). The results from ***Appendix 4—figure 4*** are summarised in ***Figure 7A*** in the main text.

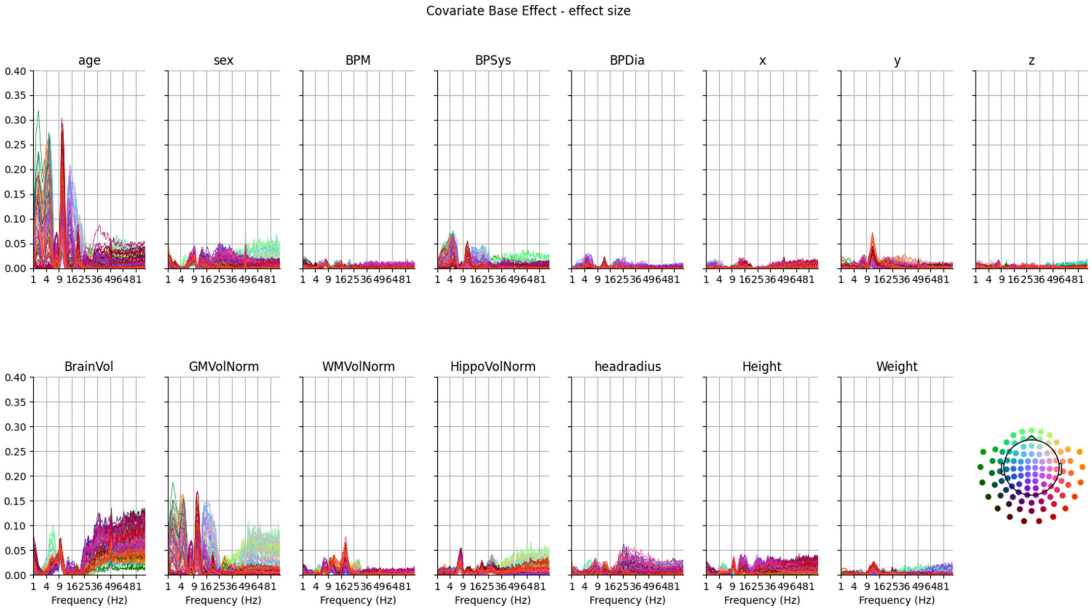
Appendix 4—figure 4 shows how the Cohen's F^2 estimates for age change between two models. The first model contains an intercept and the z-transformed ages as regressors and the second model contains the z-transformed values of an additional covariate. Cohen's F^2 for the age regressor is computed from both models, and ***Appendix 4—figure 4*** shows the difference between the two. Age itself is excluded from this analysis. This result is summarised in ***Figure 7B*** in the main text.



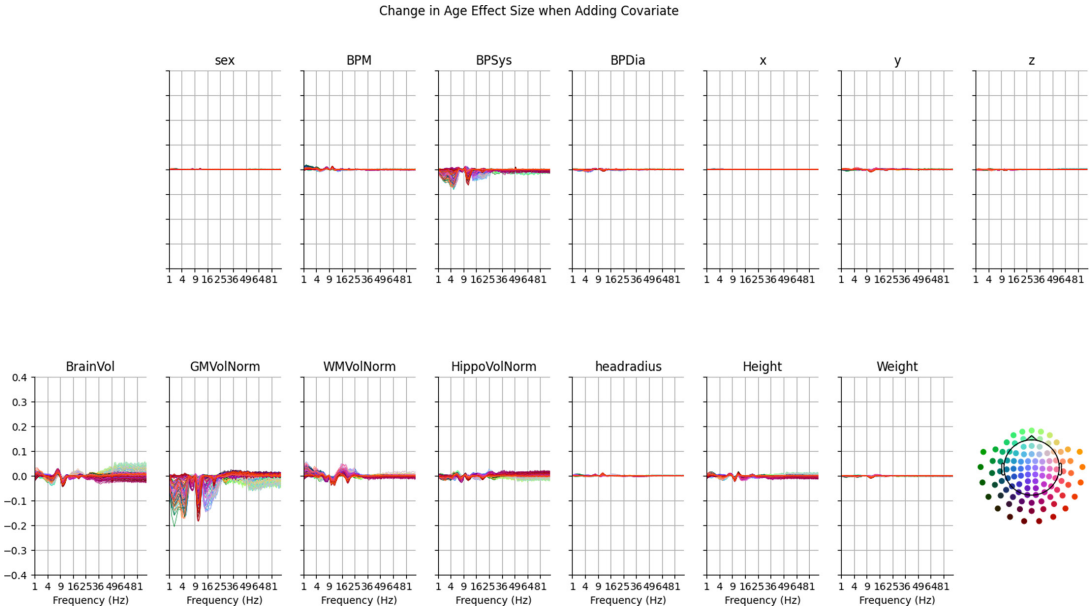
Appendix 4—figure 1. GLM-Spectrum of parameter estimates for all covariates.



Appendix 4—figure 2. GLM-Spectrum of t-statistics for all covariates.



Appendix 4—figure 3. GLM-Spectrum of effect sizes for all covariates.



Appendix 4—figure 4. GLM-Spectrum of changes in estimated age effect sizes when including a covariate in the model. Age itself is excluded from this figure.

Appendix 5

Robustness to head position correction methods

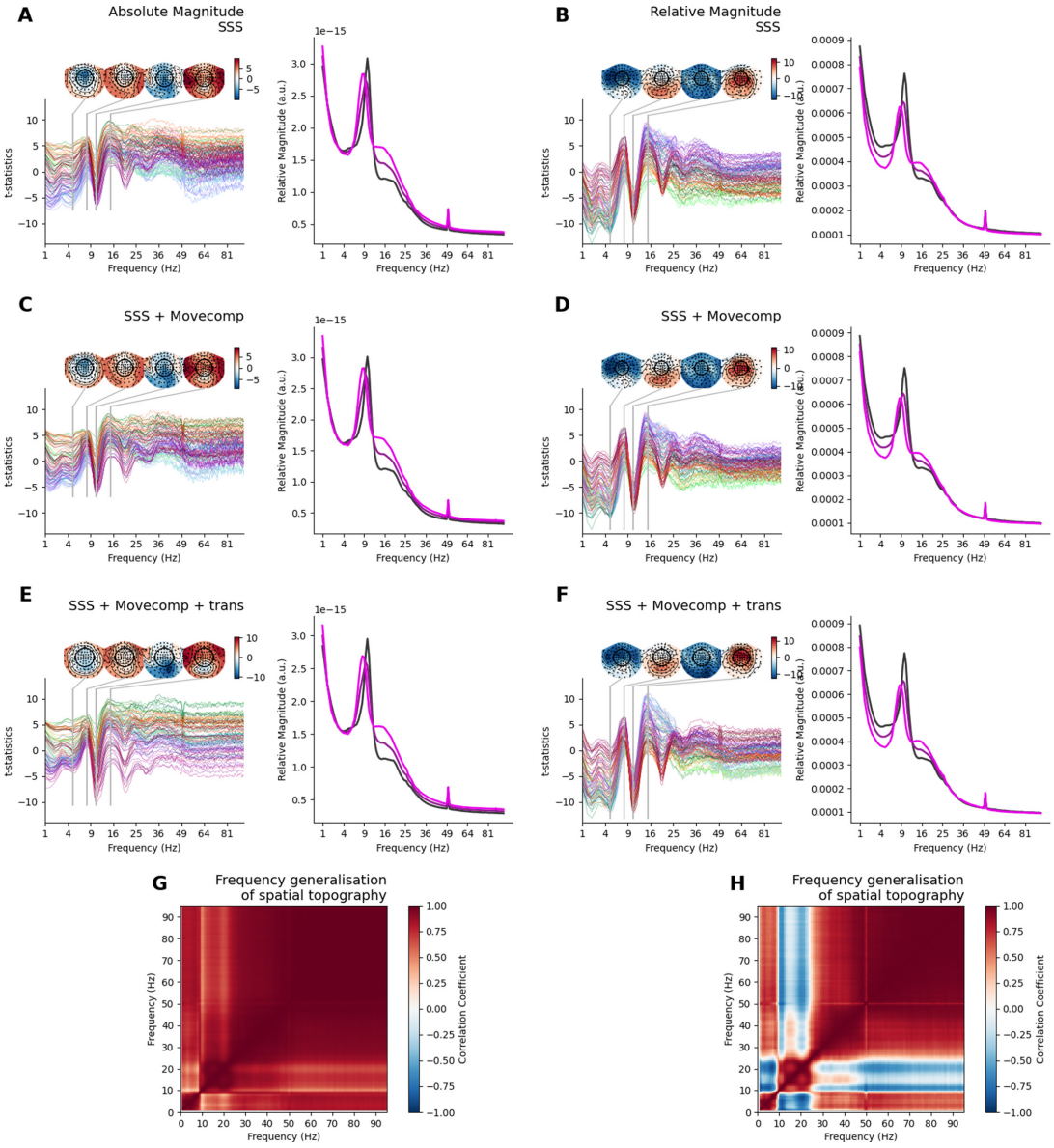
The head position of participants within the MEG sensor dewar is an important consideration that has the potential to change the signal-to-noise level of each individual data recording. There is a significant difference in head position as a function of age in the Cam-CAN dataset in Y (front-back) direction, indicating that older participants are seated further forward in the dewar than younger participants (***Appendix 5—figure 1***).



Appendix 5—figure 1. Correlations between head position and age for the Cam-CAN dataset.

Both maxfilter processing and transformation to relative power are thought to at least partially compensate for differences in head position. The change in the GLM-Spectrum with respect to head position correction is discussed in section 'Sample size planning for effects of age on the neuronal power spectrum'. The results in ***Appendix 5—figure 2*** show the full GLM-Spectra for the age effect computed for each combination of two sensor normalisation conditions – no normalisation (absolute magnitude) and z-transformed time series (relative magnitude) – and three SSS-based head position correction conditions – no correction, within recording head position correction ($-movecomp$), and within and between recording head position correction ($-movecomp$ and $-trans$). Results from the analysis of the relative magnitude with both within and between recording head position correction are shown in ***Figure 1*** of the main text. Results from the analysis of the absolute magnitude with both within and between recording head position correction are shown in ***Figure 5*** of the main text. The SSS head position correction methods have little effect on the estimated group age effect whereas the sensor normalisation changes the overall pattern of results as discussed in section 'Sample size planning for effects of age on the neuronal power spectrum'.

The impact of the sensor normalisation is a change in the spectral specificity of spatial patterns in the age effect. The largest component of the absolute magnitude age effect is a consistent spatial pattern covering the whole frequency range, leading to high positive correlations in the spatial maps of the age effect across all frequencies (***Appendix 5—figure 2G***). In contrast, spatial topography of the relative magnitude age effect varies strongly across frequency (***Appendix 5—figure 2H***).



Appendix 5—figure 2. GLM-Spectrum results showing the effect of age estimated for two different sensor normalisations and three different Signal Space Separation (SSS) head position correction types. (**A**) The age effect for the absolute magnitude with SSS applied without head position correction. (**B**) The age effect for the relative magnitude with SSS applied without head position correction. (**C**) The age effect for the absolute magnitude with SSS applied with head position correction applied within each dataset (−movecomp in maxfilter software). (**D**) The age effect for the relative magnitude with SSS applied with head position correction applied within each dataset (−movecomp in maxfilter software). (**E**) The age effect for the absolute magnitude with SSS applied with head position correction applied within each dataset (−movecomp in maxfilter software) and head position alignment to a reference datafile (−trans in maxfilter software). (**F**) The age effect for the relative magnitude with SSS applied with head position correction applied within each dataset (−movecomp in maxfilter software) and head position alignment to a reference datafile (−trans in maxfilter software). (**G**) The spectral generalisation of the topography of the absolute magnitude age effect. (**H**) The spectral generalisation of the topography of the relative magnitude age effect.

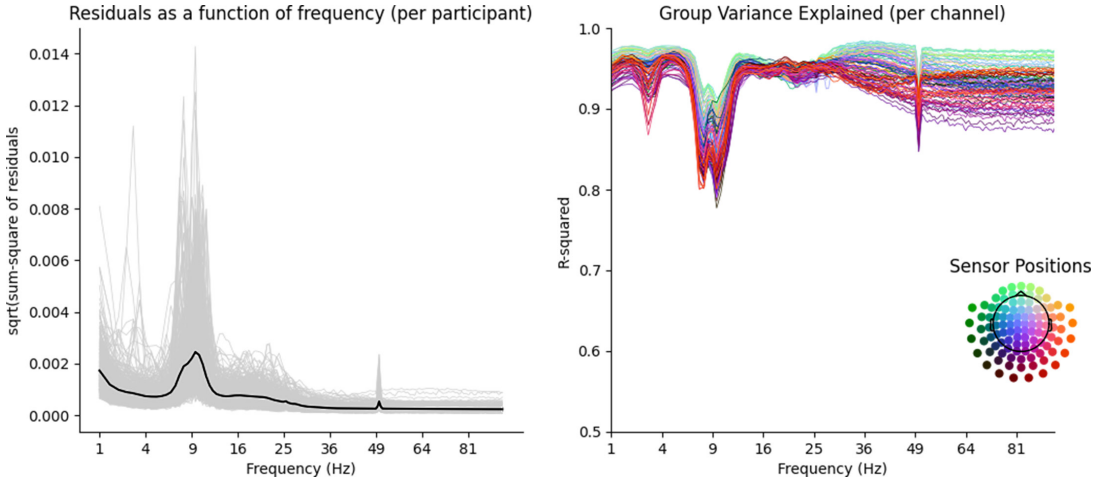
Appendix 6

Multicollinearity between age and grey matter volume

There is a strong correlation between age and GGMV (Pearson's *r*=–0.75). The shared variance arising from this collinearity adds nuance to the interpretation of the results, which we explore in more detail in this section.

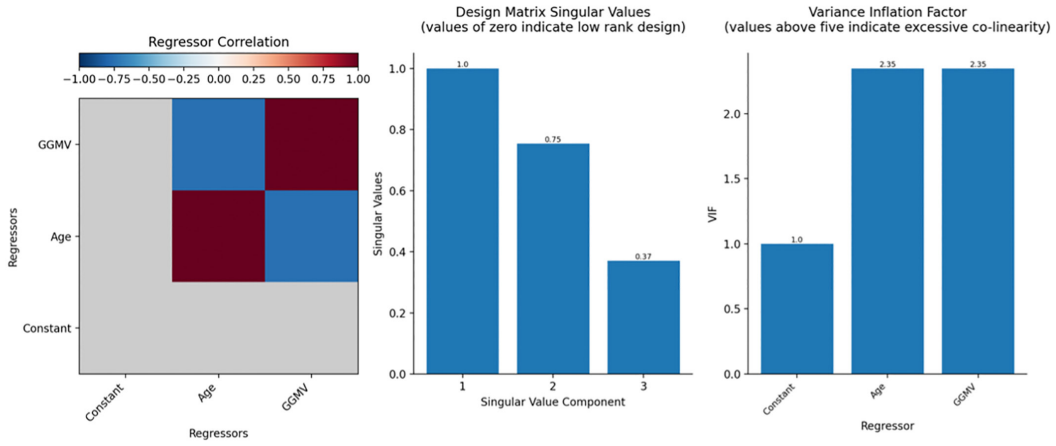
Firstly, the sum-square residuals for the group-level model fit including both age and GGMV are shown as a function of frequency in ***Appendix 6—figure 1***. We see that the residuals broadly follow the overall distribution of variance in the data, peaking at low frequencies and in the alpha range.

These frequency ranges are where the strongest signal is visible, but also the highest variability between participants. We would expect that the group model would not perform so well in the points of greatest variability. Importantly, though the residuals are relatively high in the alpha, this is still in the context of a very well-performing model with R2 values of around 80%.



Appendix 6—figure 1. Model residuals and coefficient of determination as a function of frequency for each channel show that the group model performs well. (Left) The sum-square residuals of the first level models with each individual data recording (grey lines) and the overall group average (black line). (Right) The R2 coefficient of determination for the group-level model showing that the model is able to describe a high amount of variability across both channels and frequencies.

Secondly, the correlation between age and GGMV is not inherently problematic for the GLM, but it does add complexity and nuance to the interpretation of the results. Some additional model validation statistics are shown in ***Appendix 6—figure 2***.



Appendix 6—figure 2. Model validation statistics and diagnostics for the group-level GLM containing an intercept, a z-transformed age regressor, and a z-transformed global grey matter volume (GGMV) regressor. (Left) The correlation matrix between the three regressors shows a large negative correlation between age and GGMV. (Centre) The singular values of the design matrix stay well above zero for all components, indicating that the collinearity between regressors does not cause the model fit to critically fail. (Right) The variance inflation factors for all three regressors shows peak values of 2.35, which indicates inflated variance (VIF>1). Specifically, this corresponds to an increase in standard error by a factor of 1.533.

The singular value spectrum of the design matrix indicates whether a design is low rank, the smallest singular value in this case in 0.37, which indicates that there isn't a rank deficiency which would prevent us from estimating the model.

Though we can estimate the model, correlated regressors can reduce its efficiency. The variance inflation factors for the joint AGE-GGMV model are above 1 for both parametric regressors, indicating that the standard errors of their estimates are inflated. The VIF of 2.35 indicates that the standard errors of this joint model are around sqrt(2.35) = 1.533 times greater than they would be in a separate or uncorrelated model. Though there is no hard rule for this, the literature generally suggests that a VIF above 5 (or sometimes 10) indicates severe multicollinearity.

Including additional regressors in the model can change the age estimate by 'partialling' out the variance that can be attributed to the other variables, and by inflating standard errors. In this specific case of GGMV, the partialled estimates are reduced heterogeneously across space and frequency, and the amount of inflation is at a tolerable level. Overall, the regression is able to separate the unique effects of age and GGMV, at the cost of this inflation in the associated standard errors.

Finally, the partialled effects in the GLM can already be interpreted as the 'change in Y for a 1-unit increase in X whilst all other predictors are held constant'. In our case, this is equivalent to asking 'Is there an effect of age on the MEG spectrum in a group where GGMV does not change with age'. The results show that it is not feasible to interpret changes in low-alpha separately from change in GGMV, but that a substantial component of the low-frequency, high alpha, and beta band changes are distinct from global structural change.

Appendix 7

Analysis family

Appendix 7—table 1. Summary of regression analyses performed in this article organised by figure.

Figure	Field	Specification
1, 2, 4, 9, 18, 19	Analysis	Linear effect of age (Cam-CAN)
	Dimensions	Sensors× frequency
	Model	$RelativePower = Intercept + ztrans(Age)$
	Permutations	2500
3	Analysis	Quadratic effect of age (Cam-CAN)
	Dimensions	Sensors× frequency
	Model	$RelativePower = Intercept + ztrans(Age) + ztrans(Age)^2$
	Permutations	2500
5	Analysis	Linear effect of age (Cam-CAN and MEG-UK)
	Dimensions	Sensors× frequency
	Model	$RelativePower = Intercept + ztrans(Age)$
	Permutations	2500
6, 17	Analysis	Linear effect of age (Cam-CAN)
	Dimensions	Sensors× frequency
	Model	$AbsolutePower = Intercept + ztrans(Age)$
	Permutations	2500
7, 12, 13, 14	Analysis	Linear effect of covariates (Cam-CAN)
	Dimensions	Sensors× frequency
	Model	$RelativePower = Intercept + ztrans(Covariate)$
	Permutations	2500
7, 12, 13, 14	Analysis	Linear effect of age with covariate included (Cam-CAN)
	Dimensions	Sensors× frequency
	Model	$RelativePower = Intercept + ztrans(Age) + ztrans(Covariate)$
	Permutations	2500
8, 9	Analysis	Linear effect of GGMV with age (Cam-CAN)
	Dimensions	Sensors × frequency
	Model	$RelativePower = Intercept + ztrans(Age) + ztrans(GGMV)$
	Permutations	2500
10	Analysis	Linear effect of age (Cam-CAN)
	Dimensions	Source parcels× frequency
	Model	$RelativePower = Intercept + ztrans(Age)$
	Permutations	2500
11	Analysis	Linear effect of age without ICA (Cam-CAN)
	Dimensions	Sensors× frequency

Appendix 7—table 1 Continued on next page

Appendix 7—table 1 Continued

Figure	Field	Specification
	Model	$RelativePower = Intercept + ztrans(Age)$
	Permutations	2500